Seasonal hydrology and permafrost disturbance impacts on dissolved organic matter composition in High Arctic headwater catchments 1

Julien Fouché, M. J Lafrenière, K. Rutherford, S. Lamoureux

NRC Research Press

ARTICLE

Seasonal hydrology and permafrost disturbance impacts on dissolved organic matter composition in High Arctic headwater catchments[1]

J. Fouché, M. J. Lafrenière, K. Rutherford, and S. Lamoureux

Abstract: Arctic landscapes are experiencing intense warming and modification of precipitation regimes with climate change. Permafrost disturbances and climate change impacts on hydrology of Arctic watersheds are likely to modify the quantity and composition of exported dissolved organic matter (DOM). In July 2007, intense rainfall and active layer thickening caused widespread active layer detachments at Cape Bounty, Melville Island (Canada). This study investigates the impacts of seasonal hydrology and permafrost disturbance on DOM composition exported from High Arctic headwater catchments. In 2012, streams were sampled from three disturbed catchments and one undisturbed catchment. The composition of DOM was characterized using absorbance and fluorescence spectroscopy. DOM was mostly exported during the spring freshet. Throughout this period, the undisturbed catchment exported humified DOM with high humic-like fluorescence that likely originated from runoff through shallow organic rich soil. In contrast, DOM exported from disturbed catchments was fresher, less humified with a high proportion of low molecular weight humic acid. We demonstrate that disturbed catchments delivered likely more labile DOM derived from either thawed permafrost or enhanced microbial activity. If this labile DOM comes from an ancient pool, as indicated by other studies at this site, disturbances may strengthen the permafrost carbon feedback on climate change.

Key words: active layer detachments, dissolved organic matter, fluorescence, High Arctic, parallel factor analysis, PARAFAC.

Résumé : Avec le changement climatique, les paysages arctiques connaissent un réchauffement intense et une modification des régimes de précipitation. Les impacts des perturbations du pergélisol et du changement climatique sur l'hydrologie des bassins hydrographiques arctiques vont probablement modifier la quantité et la composition de matière organique dissoute (MOD) exportée. En juillet 2007, des averses intenses et l'épaississement de la couche active ont causé des décollements généralisés de la couche active à Cape Bounty, île Melville (Canada). Cette étude examine les impacts de l'hydrologie saisonnière et de la perturbation du pergélisol sur la composition de la MOD exportée des bassins versants d'amont du Haut-Arctique. En 2012, on a échantillonné des cours d'eau de trois bassins versants perturbés et d'un bassin versant non perturbé. La composition de la MOD a été analysée en utilisant la spectroscopie à fluorescence et l'absorptiométrie. La MOD a surtout été exportée pendant la crue printanière. Pendant cette période, le bassin versant non perturbé a exporté de la MOD humifiée à haute fluorescence telle humique qui provenait probablement de ruissellement par sol riche organique mince. En revanche, la MOD exportée de bassins versants perturbés était plus fraîche, moins humifiée avec une haute proportion d'acide humique à faible poids moléculaire. Nous démontrons que les bassins versants perturbés ont déversé

Received 15 July 2016. Accepted 25 January 2017.

J. Fouché, M.J. Lafrenière, K. Rutherford, and S. Lamoureux. Department of Geography, Queen's University, Kingston, ON K7L 3N6, Canada.
Corresponding author: J. Fouché (email: julien.fouche@queensu.ca).
[1]This article is part of a Special issue entitled "Arctic permafrost systems".

de la MOD probablement plus labile provenant du pergélisol dégelé ou de l'activité microbienne améliorée. Si cette MOD labile vient d'un bassin ancien, tel que révélé par d'autres études à ce site, les perturbations peuvent renforcer la rétroaction du carbone du pergélisol sur le changement climatique.

Mots-clés : décollements de la couche active, matière organique dissoute, fluorescence, Haut-Arctique, analyse de facteurs parallèles (« PARAFAC »).

Introduction

Climate change is faster in the Arctic than elsewhere on the globe and is expected to intensify in the future (IPCC 2013). Climate models project both ground warming and increased precipitation in the High Arctic (Guido et al. 2016). Arctic rivers and particularly streams from headwater catchments exhibit a strong hydrologic seasonality with maximum discharge occurring during the spring freshet (McNamara et al. 2008; Lewis et al. 2012).

Higher rainfall and deepening of the thaw front due to warm air temperatures result in the enhancement of thermokarst activity and slope disturbances such as active layer detachments (ALDs) (Lewkowicz 2007; Lamoureux and Lafrenière 2009). Localized landscape disturbances will modify the water flow pathways, while thickening of the active layer will alter subsurface flow paths (Frey and McClelland 2009; Lamoureux et al. 2014).

Permafrost landscapes in the Arctic store ~1300 Gt of organic carbon (Hugelius et al. 2014), and the delivery of dissolved organic matter (DOM) from Arctic rivers represents a major flux of carbon to the Arctic Ocean (Hernes and Benner 2006). In Arctic rivers, most of the annual DOM flux occurs during the spring freshet (Finlay et al. 2006). DOM represents a complex mixture of organic compounds composed of terrestrial inputs and microbial products (Kalbitz et al. 2000). The composition and the biodegradability of riverine DOM are controlled by (1) the nature of vegetation and soil organic matter (Ward and Cory 2015), (2) sorption processes in soil mineral layers (Kawahigashi et al. 2006), and (3) biodegradation and photodegradation occurring within soils and rivers (Mann et al. 2012; Olefeldt et al. 2013).

Permafrost, which constrains percolation and retention of DOM in soils, leads to high concentrations of DOM in Arctic surface waters (Kawahigashi et al. 2004). Although DOM in Arctic rivers represents one of the most active pools of terrestrial carbon (Vonk et al. 2015), its fate with deeper thaw and permafrost degradation is still uncertain (Frey and McClelland 2009). It is crucial to better understand how the composition of exported DOM varies temporally and with permafrost disturbance to project the strength of the permafrost carbon feedback on climate change (Schuur et al. 2015).

Because optical properties of dissolved organic compounds depend on their weight, aromaticity, and structural configuration, spectroscopic techniques provide relevant proxies to characterize DOM. Thus, fluorescence characterization of DOM is a rapid, precise, and relatively low-cost technique that allows for extensive analysis of DOM composition (Fellman et al. 2010).

This research aims to determine the impacts of seasonal hydrology and permafrost disturbance on the composition of DOM exported from High Arctic headwater catchments using absorbance and fluorescence measurements. We collected water samples daily at stream outlets along the active hydrologic season to capture the seasonal variability of DOM composition in the Cape Bounty Arctic Watershed Observatory (CBAWO), Nunavut, Canada. Streams from undisturbed and recently disturbed headwater catchments were sampled to assess the impacts of ALDs on DOM composition. Although previous research from the CBAWO reports on the impact permafrost disturbance had on sediment fluxes (Lamoureux et al. 2014), total dissolved solute fluxes (Lafreniere and Lamoureux 2013), and sources of dissolved nitrogen (Louiseize et al. 2014), here we characterize for the first time the optical properties of DOM in four headwater catchments during an entire hydrologic

Fig. 1. Map illustrating the location of the studied catchments at the Cape Bounty Arctic Watershed Observatory (CBAWO), Melville Island (Canada). Disturbed catchments (in order of increasing disturbance) Caribou (CR), ALD 05 (ALD), and Ptarmigan (PT) were subject to active layer detachment slides in 2007 (grey polygons), while the Goose (GS) catchment remains undisturbed.

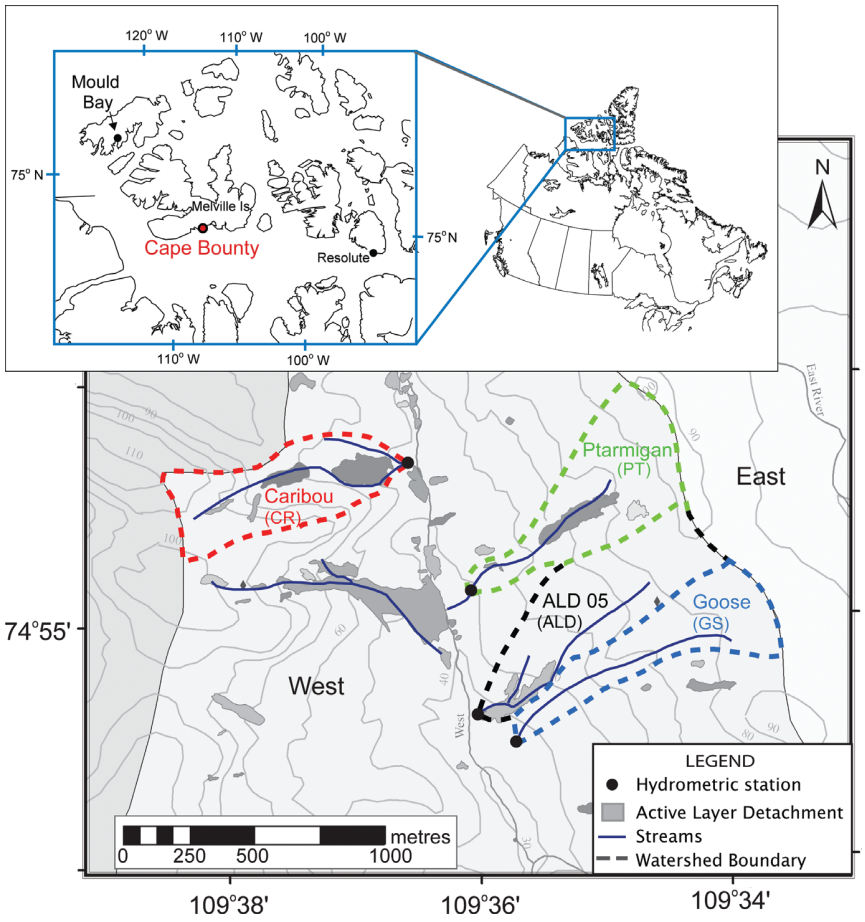

season. This study makes an important contribution to our understanding of the potential for permafrost disturbance to increase the export of fresh and low molecular weight compounds from small High Arctic streams.

Methods

Study site

Water samples were collected in four catchments in the CBAWO over the 2012 melt season. The CBAWO is situated on the south-central shore of Melville Island in the Canadian Arctic Archipelago (74°54′N, 109°35′W) (Fig. 1) and consists of adjacent unglacierized watersheds referred to as West and East (unofficial names), which both drain into small lakes similar in size.

This site is characterized by a High Arctic climate with a thaw period occurring from June to August and low precipitation. Most of precipitation falls as snow during 8–9 months (Lamoureux et al. 2014). Mean monthly July and January air temperatures are 4.0 and −33.1 °C, respectively. The mean annual precipitation recorded at Mould Bay (1971–1994) is

102 mm of snowfall and 16.3 mm of rainfall (Environment Canada 2009; Lafrenière and Lamoureux 2013). In 2012, the mean July air temperature and rainfall were 7.8 °C and 57.2 mm, respectively. The study area is characterized by continuous permafrost and the active layer thickness usually ranged from 50 to 70 cm (Lafrenière et al. 2013).

The landscape consists of unconsolidated marine and glacial sediments that cover devonian sandstones and siltstones (Hodgson and Vincent 1984). Soils are typical cryosols with a thin organic horizon (<5 cm) overlying unaltered parent material (Cockburn and Lamoureux 2008). The vegetation is characterized by patchy low tundra and consists of wet, mesic, and polar desert communities dominated by prostrate dwarf-shrub, graminoïds, and mosses (Atkinson and Treitz 2012). Slopes are gentle and drainage is typically characterized by simple patterns such as shallow channels, diffuse flow, or sheet flow over saturated ground (Lamoureux and Lafrenière 2009).

Exceptionally warm air temperatures in July 2007 resulted in thickening of the active layer and extensive ground ice melt, which together with an intense mid-July rain event caused the development of widespread ALDs across the West River watershed (Lamoureux and Lafrenière 2009). ALDs are shallow and large slope failures that move soil along the base of the active layer up to 300 m downslope (French 2007). These mass movements in CBAWO, which vary widely in size from <100 to 53 800 m^2, contain fragmented soil and vegetation mixed with underlying marine clays (Lamoureux and Lafrenière 2009). ALDs create specific geomorphic features such as steep head scarps with many tension cracks, fractured blocks, and compressed and overturned soil ridges (Lamoureux and Lafrenière 2009; Lafrenière and Lamoureux 2013).

In 2012, four headwater catchments within the West River watersheds were selected to examine the impact of seasonal hydrology and ALD on the composition of exported DOM by High Arctic rivers (Fig. 1). Two of these catchments, Goose (GS) and Ptarmigan (PT), have been monitored prior to any recent disturbance in 2007. Investigations in the ALD 05 (ALD) and Caribou (CR) catchments began in 2008 and 2009, respectively. All catchments are similar in term of size, hydrology, geology, slope, soil, and vegetation cover (Lamoureux et al. 2014). Goose has never experienced any physical disturbance and represents an undisturbed control for comparison. Caribou, ALD, and Ptarmigan represent increasing extent area of disturbance and channel density (Lamoureux et al. 2014). Caribou and ALD are moderately disturbed (Caribou: disturbed area = 12.4%, channel density = 6.4%; ALD: disturbed area = 6.3%, channel density = 11.0%). In Ptarmigan, which represents the most disturbed catchment, ALDs occupy ~11.8% and the channel density represents 15.2% of the total catchment area (Lamoureux et al. 2014). Intensity and duration of snowmelt runoff depend on topographic conditions that allow for snow accumulation and drainage. Stream flow significantly varies among catchments, as exhibited by significantly lower discharge in ALD than in Goose, Caribou, and Ptarmigan. The surface runoff in Goose and Caribou occurs as diffuse flow in poorly incised, vegetated channel, and water tracks. ALD is drained by a fragmented channel and flow distance downstream of disturbance is minimal (Lamoureux et al. 2014). Ptarmigan is drained by an incised channel that flows into mineral soils through the length of the two elongate disturbances. In Ptarmigan, disturbances are well connected to downstream; thus, the water delivered provides important information on ALD impacts on stream DOM properties and biogeochemical functioning (Lamoureux et al. 2014; Louiseize et al. 2014)

In all catchments, river discharge typically lasts from early June until mid- to end of July. Early June, the river flow, which peaks within few days and recedes rapidly, is sustained by snowmelt from snowpacks located in channels and depression. In the lack of both significant rainfall and groundwater baseflow, streams usually dry up in July. After the nival melt, stream flow is only rejuvenated by rainfall events that are infrequent and of low magnitude (Lafrenière and Lamoureux 2013).

Fig. 2. Mean hourly discharge (*Q*) from June to July 2012 in (A) Goose, (B) Caribou, (C) ALD, and (D) Ptarmigan and daily cumulative rainfall on the West watershed. The grey area highlights the nival melt. Note the differences in scale for discharge between catchments.

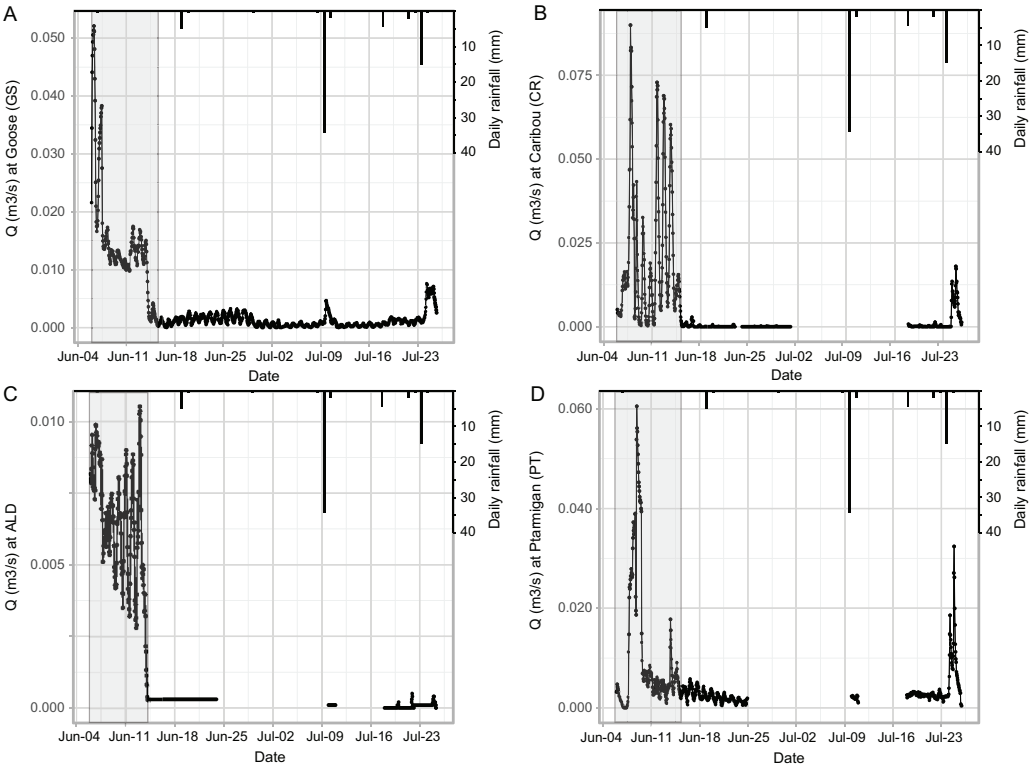

Hydrologic regimes

The methods of discharge and precipitation measurements are detailed in Louiseize et al. (2014). As reported by Louiseize et al. (2014), seasonal hydrographs for Goose, Caribou, ALD, and Ptarmigan were divided into nival melt (or spring freshet), baseflow, and stormflow phases depending on changes in discharge and the frequency of rainfall (Fig. 2). For all catchments, the nival melt period began on June 5 and this was determined to have transitioned into baseflow on June 14 in ALD and on June 16 in Goose, Caribou, and Ptarmigan. The baseflow period ceased with the end of stream flow on June 24 in ALD and Ptarmigan and on July 1 in Goose and Caribou. Precipitation events generated stormflow runoff periods from July 9 to July 10 in Goose, ALD, and Ptarmigan and from July 18 to 25 in all streams, respectively referred to as first and second stormflow events (Fig. 2).

Field sampling

Water sampling was conducted over the three hydrologic phases of the hydrologic season from the first day of flow on June 5–25. The sample collection and preparation are detailed in Louiseize et al. (2014). Water samples were collected at stream outlets twice daily at approximately 10:00 (i.e. minimum daily discharge) and 18:00 (i.e. maximum daily discharge) during the nival melt and stormflow periods and once daily at approximately 18:00 during baseflow. Suspended sediment concentration (SSC) and seasonal specific yield measurements and calculation are detailed in Lamoureux et al. (2014). After sample collection using 1 L Nalgene rinsed bottles, bottles were completely filled and were kept

cool in the dark until filtration (typically within 30–120 min). Samples for dissolved ion analysis were filtered through 0.22 μm PVDF membrane filters. New filters were used for each sample. They were stored in HDPE pre-cleaned vials, rinsed with filtered sample, and filled with no headspace. Samples were refrigerated until analysed for dissolved ion analysis at Queen's University.

Water samples for dissolved organic carbon (DOC) and total dissolved nitrogen (TDN) and optical analyses were filtered through pre-combusted 0.7 μm glass fiber filters (GF/F, Whatman) with a glass filtration apparatus. DOC and TDN samples were stored acidified at pH 2 in 45 mL amber EPA vials with Teflon-lined septa and refrigerated in the dark until analysed at Queen's University.

Dissolved organic and inorganic solute analyses

All of the organic and optical measurements were conducted in the Department of Geography and Planning at Queen's University. DOC and TDN measurements were performed simultaneously using high-temperature combustion on a Shimadzu (TOC-V) organic carbon analyser with a nitrogen chemiluminescence detection unit (Shimadzu TMN-1). Milli-Q blanks were run at the beginning and throughout every run to ensure consistency. A new calibration was generated for each DOC and TDN run and based on replicate analyses of standards, which were analysed within every run, analytical errors for DOC and TDN were 2.9% for DOC measurements and 2.3% for TDN measurements (Louiseize et al. 2014). DOC and TDN were calculated as the mean of between three and five injections with the coefficient of variance always <2%. Dissolved organic nitrogen (DON) was determined as the difference between TDN and dissolved inorganic nitrogen (DIN), which corresponds to the sum of the nitrogen mass from NH_4^+, NO_3^-, and NO_2^- (when detectable).

Dissolved inorganic anions and cations were analysed by liquid ion chromatography with a Dionex ICS-3000. Anions were measured using KOH eluent with a gradient elution of 11–40 mmol L^{-1} KOH flowing at 1.0 mL min^{-1} through an AS18 analytical column and an ASRS 300 suppressor. Detailed method detection limits and precision are described in Louiseize et al. (2014). Concentrations of NH_4^+ were measured by colorimetry using an Astoria Pacific FASPac II flow analyser. The detection limit was <0.01 ppm N and the analytical error was 0.9%. We calculated the total dissolved solute (TDS) concentration in mg L^{-1} as the sum of all ion concentrations.

DOM optical indices and PARAFAC modeling

UV-visible absorbance and fluorescence measurements and emission excitation matrices (EEMs) were collected at room temperature using a Horiba Aqualog. Each sample was run individually in a 1 cm path length quartz cuvette. Absorbance spectra were blank-corrected using Milli-Q water. UV-visible absorbance spectra and excitation values were collected between 240 and 600 nm at 3 nm intervals and emission wavelengths were scanned from 214.16 to 621.03 nm at 3.15 nm intervals. The samples were run at varied integration time and gain settings to optimize the quality of the results for each sample. EEM files were corrected for blanks and inner filter effects (McKnight et al. 2001) and first- and second-order Rayleigh scatter effects were removed using the manufacturer's correction procedure. The signal was normalized using a 1 ppm quinone sulfate standard, made up in 0.05 mol L^{-1} H_2SO_4, and run daily during measurements to account for fluctuations in the instrument light source characteristics. All intensities were reported in terms of quinone sulfate units.

Eight optical indices from absorban (Walker et al. 2013) and fluorescence spectra (Fellman et al. 2010) were calculated and PARAFAC modeling was performed (Stedmon et al. 2003) to characterize DOM.

Absorbance data were converted to Napieran absorption coefficients (E in m^{-1}) by multiplying raw absorbance values by 2.303 and dividing by the cuvette path length (m)

(Hu et al. 2002). The absorption coefficient at 350 (E350) was calculated and represents a quantitative measure of the chromophoric fraction of DOM that is positively correlated with DOC and lignin phenol content (Spencer et al. 2009; Laurion and Mladenov 2013; Mann et al. 2016). Specific UV absorbance ($SUVA_{254}$, L mg^{-1} C m^{-1}) was calculated as the decadal UV absorbance at 254 nm (m^{-1}) divided by the DOC concentration (mg C L^{-1}) (Weishaar et al. 2003). $SUVA_{254}$ is positively correlated with bulk DOM aromaticity because aromatic compounds absorb more light in the UV-visible spectra. Because plant and soil organic matter is composed of tannin substances and humic acids, terrestrially derived DOM shows higher aromaticity than autochtonous and microbially derived DOM. Absorption spectra slopes were calculated over two spectral bands, 275–295 nm (S_{295}) and 350–400 nm (S_{400}), and the slope ratio (S_R) was calculated as the ratio between the two spectral slopes (Helms et al. 2008). Slope coefficients, which differ between DOM sources, have been reported to be indicators of molecular weight and aromaticity. Higher slope coefficients are associated with lower molecular weight and decreasing DOM aromaticity (i.e., more degraded and (or) microbial source) (Helms et al. 2008; Mann et al. 2012; Laurion and Mladenov 2013; Frey et al. 2015).

The fluorescence index (FI), which was calculated as the ratio of emission at 470–520 m at an excitation wavelength of 370 nm (McKnight et al. 2001; Cory et al. 2010), indicates the dominant source of DOM from terrestrially derived (plant and soil organic matter, ~1.2) to microbial (extracellula release and leachate from bacteria and algae, ~1.8) (Fellman et al. 2010). The freshness index (BIX) is calculated as the ratio of emission at 380 nm divided by the emission intensity maximum observed between 420 and 435 nm at an excitation wavelength of 310 nm (Parlanti et al. 2000). BIX is an indicator of the relative freshness of the bulk DOM, increasing with more recently derived DOM (Fellman et al. 2010). The humification index (HIX), which indicates the humic substance content or extent of humification, was calculated as the area under the emission spectra 435–480 nm divided by the peak area over two spectral bands,, 300–345 and 435–480 nm, at an excitation of 254 nm (Ohno 2002).

PARAFAC models decompose data that are arranged in three-dimensional arrays (sample × excitation wavelength × emission wavelength) into accurate spectra and relative concentrations of known fluorescent groups showing similar chemical composition in a complex DOM mixture (Murphy et al. 2008, 2013). PARAFAC individual components refer to groups as "humic-like", "fluvic-like", or "protein-like" with various properties rather than pure organic molecules.

PARAFAC modeling was performed using the DOMFLuor toolbox within MATLAB (Stedmon and Bro 2008) in order to decompose EEMs into independent fluorescent components. Excitation wavelengths below 260 nm and emission wavelengths below 312.95 were removed from matrices in order to avoid deteriorating signal-to-noise ratios (Stedmon et al. 2003). Prior to modeling, regions of the spectra influenced by first- and second-order scatter peaks and with no fluorescence (i.e., emission << excitation) were cut and replaced by missing values. A five-component model was generated incorporating a total of 199 samples from the four streams and from a few ponds and subsurface seepage sites within the catchments. Samples from the ponds and seepage sites were included in order to compare the character of DOM from these different hydrological settings with the DOM in runoff. Model parameters were constrained to be non-negative. The model, which identified components with unimodal emission maxima, was validated using residual analysis characterized by instrument noise and a lack of systematic pattern, split-half analysis, and random initialization (Stedmon and Bro 2008; Murphy et al. 2013). It explained 99.9% of the fluorescence signature.

Identified component emission and excitation loadings were compared with the open fluorescence database (openfluor.org, 53 PARAFAC models) and with previous studies using PARAFAC analysis that are not included in the database. All components have been

previously reported both in 20 independent studies from openfluor database in various environments (Tucker congruence coefficient >0.95) and in many studies in Arctic ecosystems.

Statistical analyses

All statistical analysis were carried out using the R free software version 3.2.1 (R Core Team 2013). For each sample, PARAFAC component intensities were normalized to the sum of component fluorescence intensities and expressed as their relative contribution to the total fluorescence (%). Pearson pairwise correlations were employed to determine relationships between PARAFAC components and absorbance and fluorescence indices and biogeochemical variables for the four streams along the entire hydrologic season. Two-way ANOVAs were conducted to determine the significance of spectral measurements and PARAFAC results between hydrologic phases and degrees of permafrost disturbance among catchments.

A principal component analysis (PCA) was performed to explore relationships between PARAFAC components, optical properties, discharge, SSC, and biogeochemical composition and better understand stream water composition across the hydrologic season and depending on ALD impact. Before performing the PCA, autoscaling was conducted on all variables with the FactoMineR package in order to decrease the leverage of high values.

Results

Hydrology

Although the pattern of seasonal runoff was similar for all streams, both the discharge amount and the relative contribution of each hydrologic phase varied substantially between catchments due to differences in initial snow cover thickness, channel development, and standing water (Lamoureux et al. 2014). The seasonal discharge was the highest in Goose and the lowest in ALD (Table 1). For all catchments, most of the seasonal discharge, from 64% in Ptarmigan to 94% in ALD, occurred during the nival melt (Table 1). Stream flow strongly decreased and ceased in ALD and Ptarmigan a week earlier than in Caribou and Goose (Fig. 2). Flow in Goose and Caribou was sustained due to residual snowpacks and wetter soils (Louiseize et al. 2014). A rainfall event of 35.8 mm on July 9–10 slightly regenerated stream flow in Goose, ALD, and Ptarmigan (Fig. 2). Because soils were wetted by the July 9–10 event, the second rainfall event of 8.6 mm from July 18 to 25 significantly increased all streams' discharge. Thus, this second stormflow phase represents a significant contribution of the total discharge, reaching 15% in Goose and 21% in Ptarmigan (Table 1).

Major ions and organic solute concentrations

Solute concentrations were significantly higher in disturbed catchment streams than in undisturbed catchment streams ($F = 15.1$, $p < 0.001$) (Table 1). TDS was almost six times higher in Ptarmigan (247.32 mg L^{-1}) than in Goose (39.64 mg L^{-1}). In the undisturbed Goose, the TDS concentrations increased at the end of the stormflow (Fig. 3A). In the moderately disturbed Caribou and ALD, TDS slightly increased during the onset of the stormflow and peaked during the second rainfall event (Table 1; Fig. 3A). In Ptarmigan, TDS increased throughout the season, from the end of the nival flow until the end of the stormflow period, when TDS decreased rapidly (Fig. 3A).

Seasonal DOC concentration was higher in the undisturbed Goose stream relative to disturbed catchments ($F = 14.04$, $p < 0.001$) (Table 1). DOC concentrations in the disturbed catchments Caribou, ALD, and Ptarmigan were all similar at around 3.50 mg L^{-1} over the study period. For all catchments, DOC concentration quickly declined over the first days of the nival melt, prior to peak discharge, and continued to steadily decline until the

Table 1. Seasonal yields of discharge and DOC fluxes, mean concentrations of TDS, DOC, TDN, DON, DIN, and N-NO_3^- for the entire season and during the nival melt, baseflow, and stormflow periods in Goose, Caribou, ALD, and Ptarmigan.

	Discharge (mm)	DOC flux (kg)	TDS (mg L^{-1})	DOC (mg L^{-1})	DON (mg L^{-1})	DIN (mg L^{-1})	N-NO_3^- (ppb)
Goose							
Seasonal	79.985	155.64	39.64±31.81	5.60±2.79	0.23±0.15	0.05±0.03	1.9±2.8
Nival melt	67.520	145.37	36.70±9.28	4.98±2.31	0.16±0.06	0.06±0.04	2.4±4.0
Baseflow	5.287	3.68	24.00±5.48	4.07±0.69	0.16±0.04	0.04±0.03	2.1±2.2
Stormflow	7.178	6.58	66.68±52.65	9.67±2.18	0.49±0.13	0.06±0.02	0.9±1.5
Caribou							
Seasonal	65.954	111.82	107.91±161.96	3.28±1.48	0.16±0.07	0.02±0.03	7.7±0.6
Nival melt	61.649	110.60	25.52±3.50	3.76±1.72	0.17±0.08	0.02±0.03	17.7±29.9
Baseflow	0.392	0.96	32.71±4.72	2.26±0.34	0.12±0.05	0.01±0.02	0.9±1.8
Stormflow	3.912	0.26	356.13±166.85	4.75±0.68	0.22±0.05	0.05±0.03	0.7±0.8
ALD							
Seasonal	16.012	32.07	72.61±120.08	3.74±1.73	0.20±0.09	0.02±0.02	3.9±9.5
Nival melt	15.121	30.93	29.42±8.94	4.61±1.77	0.21±0.09	0.03±0.02	8.2±13.1
Baseflow	0.718	1.06	30.86±6.61	2.62±0.19	0.18±0.07	0.01±0.02	0.4±0.8
Stormflow	0.174	0.09	270.55±194.33	6.95±0.60	0.40±0.00		
Ptarmigan							
Seasonal	63.760	54.52	247.32±258.99	3.06±2.13	0.14±0.13	0.11±0.10	64±85
Nival melt	41.440	41.67	67.38±28.05	2.98±2.11	0.12±0.11	0.10±0.05	44±42
Baseflow	8.170	4.85	164.19±57.69	1.73±0.17	0.08±0.02	0.05±0.02	18±14
Stormflow	14.150	8.01	637.29±174.27	6.21±1.04	0.35±0.13	0.30±0.14	149±121

Note: Concentrations of N-NO_3^- in Goose and Ptarmigan were published in Louiseize et al. (2014); ± refers to 1 standard deviation from the mean.

baseflow phase (F = 56.02, $p < 0.001$) (Fig. 3B). DOC reached peak concentration during the stormflow after the first rainfall event (Fig. 3B).

For all streams, the DON dominated TDN concentration, representing from 54% in Ptarmigan to 91% in ALD. DON concentration was slightly higher in the undisturbed Goose than in the disturbed catchments (F = 5.33, p = 0.002) (Table 1). In all streams, DON reached maximum concentration during the stormflow phase (F = 5.68, p = 0.02) (Table 1). DOC and DON concentrations were highly correlated (r = 0.82, $p < 0.001$) and followed the same patterns over the hydrologic season although a quick increase in DON was observed during the onset of the baseflow phase (Fig. 3C). Although DIN concentrations were greater during the stormflow in all streams, they were not correlated with DON (r = 0.19, p = 0.015) (Fig. 3D). In the most disturbed and channelized catchment, Ptarmigan, DIN concentration, and particularly NO_3^-,exceeded that of all other streams during the entire hydrologic season and particularly during the stormflow (F = 9.34, $p < 0.001$) (Table 1; Fig. 3D). Inorganic nitrogen species dynamics in Goose and Ptarmigan are detailed in Louiseize et al. (2014).

Fluorescence characterization by PARAFAC modeling

The five fluorescent components that were identified by the PARAFAC model were related to previously identified DOM fractions from various environments including from Arctic surface waters (Table 2). Each component displayed wide and smooth emission spectra with only one maximum and excitation spectra with one or two maxima (Fig. 4). Components C1, C2, and C4 have been previously related to humic-like components originating from terrestrial sources such as plant and soil organic matter, while component C3 has been referred

Fig. 3. Concentrations of (A) total dissolved solutes (TDS), (B) dissolved organic carbon (DOC), (C) dissolved organic nitrogen (DON), and (D) dissolved inorganic nitrogen (DIN) over the discharge period 2012. The grey area highlights the nival melt in the four streams.

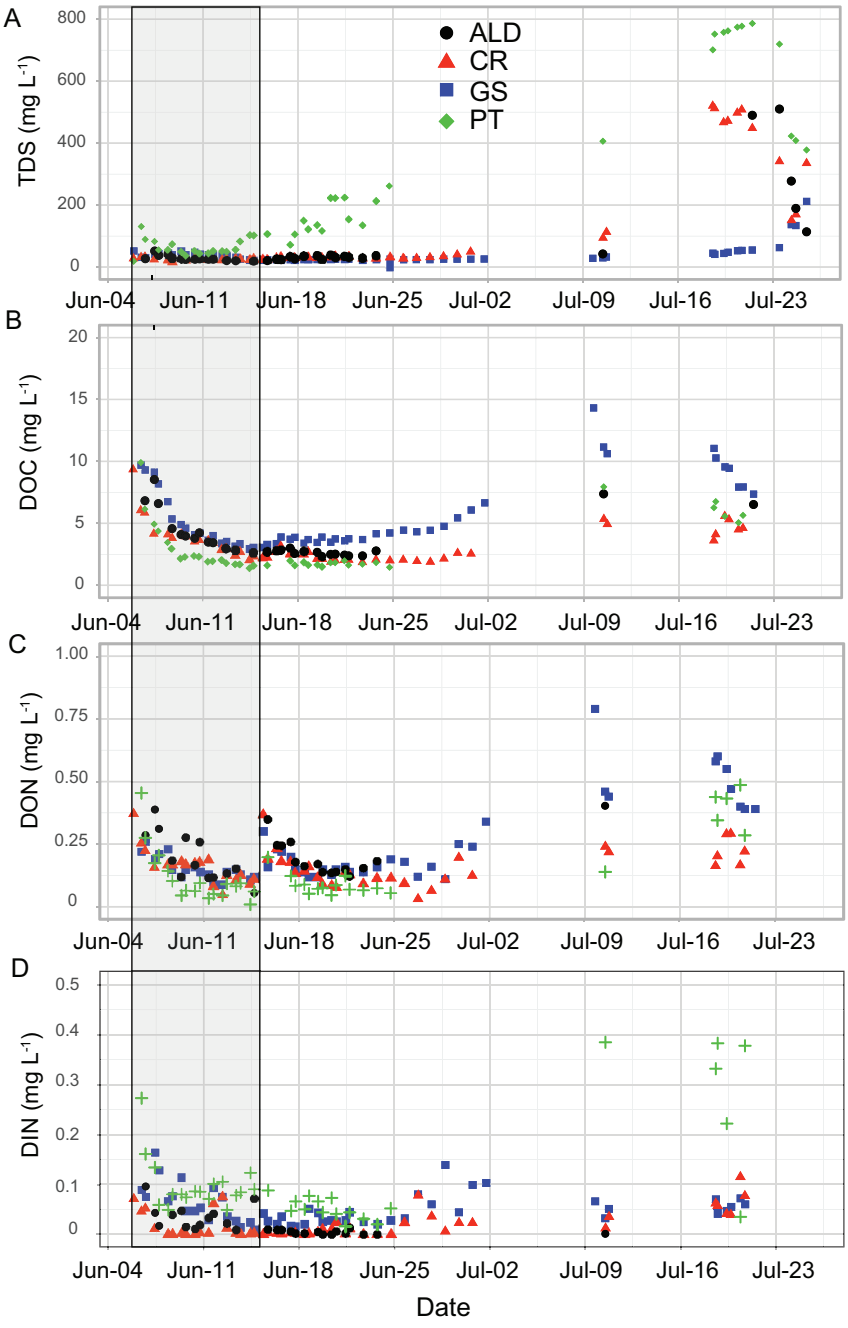

to as a humic-like component derived from microbial activity and is ubiquitous to a wide range of environments (Fellman et al. 2010). Component C5 resembles a protein-like component derived from terrestrial, marine, or autochthonous sources (Fellman et al. 2010).

Table 2. Spectral characteristics and description of the five components identified by PARAFAC and compared to previously identified components.

Component	Excitation maximum (nm)	Emission maximum (nm)	Description and likely structure	Cory and McKnight 2005	Fellman et al. 2010	Mann et al. 2016	Source of DOM
C1	<260 (380)	463	UVC humic-like; high molecular weight and aromatic humic acid	SQ2	C7	AG1	Terrestrial
C2	330	447	UVC humic-like; high molecular weight	Comp 1	C10	AG3	Terrestrial
C3	<260 (310)	395	UVA humic-like or fulvic-like; low molecular weight, common in marine environments associated with biological activity	Q3	C4	AG5	Terrestrial, autochtonous, marine
C4	312	522	Semiquinone-like; high molecular weight and highly aromatic	SQ1			Terrestrial
C5	282	332	Tryptophan-like; amino acid, soluble bound microbial DOM, tryptophan-like aromatic protein	Comp 8	C2	AG7	Terrestrial, autochtonous, marine

Note: Secondary excitation maxima are given in parentheses.

Component C1 exhibited an excitation maximum at <250 nm with another additional maximum at 380 nm (Table 2). C1 emission spectra had a maximum at a high wavelength (~463 nm), indicating the presence of relatively high molecular weight (HMW) and highly aromatic humic-like organic compounds (Table 2) (Fellman et al. 2010). C1 corresponds to a UVC humic-like component according to Fellman et al. (2010) and to a semi-quinone component in Cory and McKnight (2005). Component C2 displayed an excitation maximum at 330 nm and a relatively sharp emission peak at 447 nm (Fig. 4). This component also corresponds to UVC humic-like pool with HMW, similar to C1 but shifted to a higher excitation maximum and a lower emission maximum (Fig. 4). Component C3 has two excitation peaks, one at 260 nm and the other at 310 nm, and a relatively sharp emission maximum at 395 nm (Fig. 4). Emission that occurs at short wavelengths indicates the presence of relatively low molecular weight (LMW) and low aromatic humic acids (Fellman et al. 2010; Cory and Kaplan 2012; Vonk et al. 2013*b*; Mann et al. 2016). Components identical to C3 have been previously described as UVA humic-like components associated with biological activity (Table 2). Component C4 exhibited a wide excitation maximum at 312 nm and an emission peak at 522 nm (Fig. 4). C4, which has not been previously reported in the openfluor database, displayed an emission spectrum at longer wavelengths, indicating that this component likely contains highly aromatic molecules with very HMW compounds (Cory and McKnight 2005; Laurion and Mladenov 2013). In Cory and McKnight (2005), this component corresponds to semiquinones (SQ1). Component C5 exhibited an excitation peak at 282 nm and an emission maximum at lower wavelength (332 nm) corresponding to tryptophan-like fluorescence (Table 2). This fluorescent group represents amino acids, soluble bound microbial DOM, and more aromatic protein than tyrosine-like components (Murphy et al. 2008; Fellman et al. 2010).

As explained by Murphy et al. (2008), ratios between the intensities of different components may provide more meaningful information about DOM origin than absolute component intensities. In order to better understand DOM sources, we calculated the normalized

Fig. 4. Representative emission excitation matrices (EEMs) of each component extracted from PARAFAC modeling and identified in the four streams. The contour plots of components C1–C5 are ordered by decreasing contribution, with emission wavelength on the *y*-axis, with excitation wavelength on the *x*-axis, and shading representing the relative intensity of emission. Components 1 and 2 correspond to high molecular weight UVC humic-like components, component 3 represents a low molecular weight UVA humic-like component, component 4 refers to semiquinone, and component 5 corresponds to a tryptophan-like component.

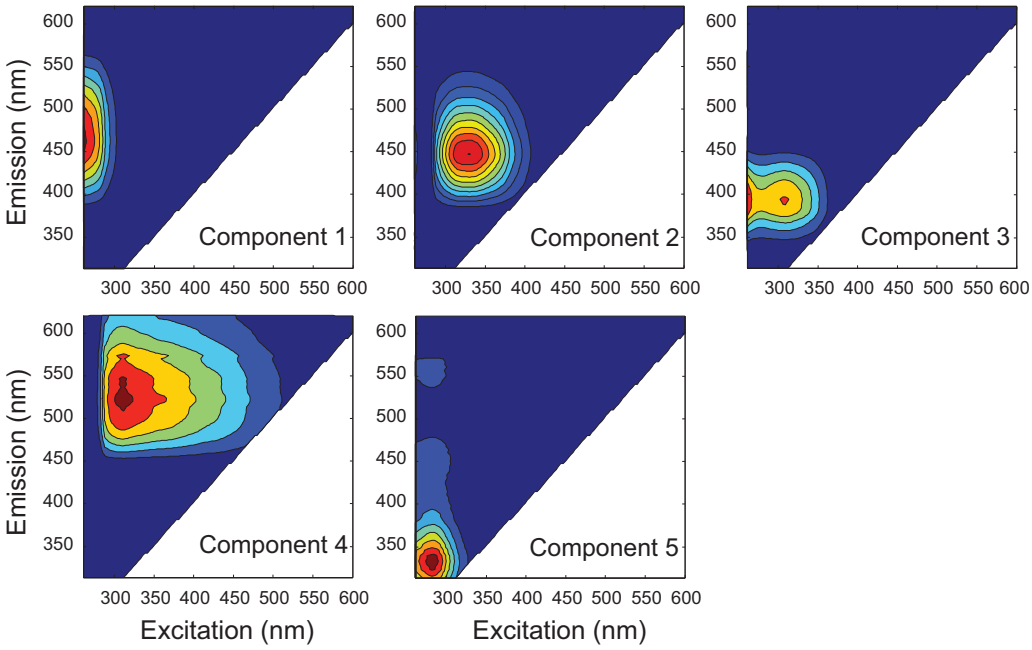

ratios of C3 to C5 (C3:(C3 + C5)), which are both related to microbial activity. Based on Cory and McKnight (2005), we also calculated the fluorescence ratio between the most aromatic humic-like components C4 and C1 (C4:(C4 + C1)) to better characterize the properties of DOM from terrestrial inputs.

DOM optical properties

E350 is an indicator of the chromophoric organic matter proportion and is strongly correlated with DOC and lignin phenol concentrations. The seasonal mean of E350 ranged from 7.9 m^{-1} in Ptarmigan to 18.7 m^{-1} in ALD and was 13.7 m^{-1} in Goose (F = 27.82, $p < 0.001$) (Table 3). Runoff in ALD exhibited high values of E350 despite relatively low DOC concentration, which contradicts previous work indicating that E350 and DOC should be strongly correlated (Walker et al. 2013; Frey et al. 2015; Mann et al. 2016). In Goose and Ptarmigan, DOC and E350 were strongly correlated (GS: $r = 0.86$, $p < 0.001$; PT: $r = 0.91$, $p < 0.001$). This relationship was weaker in Caribou ($r = 0.63$, $p < 0.001$) and particularly in ALD ($r = 0.45$, $p = 0.008$).

Seasonal $SUVA_{254}$ averaged from 3.70 in Goose to 6.59 L mg^{-1} C m^{-1} in ALD (Table 3) and showed higher values in moderately disturbed catchments Caribou and ALD, indicating a more aromatic organic matter pool ($F = 49.33$, $p < 0.001$). ALD exhibited high $SUVA_{254}$ values during the baseflow period (Table 3) and a weak correlation between absorption coefficient and DOC, which may illustrate an alteration of the absorbance signal in low wavelengths. According to the linear model developed by Weishaar et al. (2003), the aromatic carbon content approximated 27%–46% of the bulk DOC concentrations. The temporal pattern of $SUVA_{254}$ values varied among catchments (Fig. 5A). In the four catchments, $SUVA_{254}$ increased during nival melt. While $SUVA_{254}$ values remained steady during the baseflow

Table 3. Mean values of optical indices and relative contribution to total fluorescence of the five parallel factor analysis (PARAFAC) components throughout the entire season and during the nival melt, baseflow, and stormflow periods in Goose, Caribou, ALD, and Ptarmigan.

	Optical measurements								PARAFAC modeling (% relative contribution)				
	E350 (m^{-1})	$SUVA_{254}$ (L mg^{-1} C m^{-1})	S_{295} (10^{-3} nm^{-1})	S_{400} (10^{-3} nm^{-1})	S_R	FI	BIX	HIX	1st component	2nd component	3rd component	4th component	5th component
Goose													
Seasonal	13.7±5.5	3.70±0.68	13.4±0.7	16.3±0.7	0.82±0.03	1.43±0.05	0.50±0.04	0.94±0.03	41.7±2.5	25.7±0.6	17.8±1.4	9.7±1.0	4.9±3.5
Nival melt	12.2±6.7	3.33±0.57	13.2±0.3	15.8±0.5	0.83±0.02	1.41±0.02	0.48±0.02	0.93±0.03	41.2±3.2	25.9±0.4	16.9±0.9	9.8±0.8	6.1±4.6
Baseflow	12.3±2.0	4.36±0.14	12.9±0.2	16.2±0.5	0.80±0.02	1.41±0.02	0.49±0.02	0.95±0.02	43.5±1.5	25.7±0.8	17.4±0.4	10.5±0.5	2.9±2.5
Stormflow	17.7±5.1	3.19±0.51	14.3±0.6	17.0±0.5	0.84±0.02	1.50±0.03	0.56±0.03	0.92±0.01	40.0±0.9	25.5±0.4	19.7±1.0	8.5±0.7	6.3±0.9
Caribou													
Seasonal	9.2±3.1	4.28±0.94	14.0±1.8	16.2±1.5	0.87±0.06	1.45±0.06	0.51±0.06	0.92±0.02	41.8±2.0	25.1±0.8	18.2±1.4	9.5±1.0	5.3±2.7
Nival melt	9.7±7.7	4.12±1.13	14.2±2.4	15.6±1.5	0.91±0.09	1.44±0.04	0.45±0.05	0.93±0.03	43.2±2.4	25.8±1.0	17.5±0.3	10.0±0.7	3.5±3.4
Baseflow	7.7±1.1	4.81±0.31	13.0±0.3	15.7±0.5	0.83±0.02	1.41±0.02	0.52±0.02	0.92±0.02	41.8±1.2	24.6±0.6	17.5±0.4	10.0±0.3	6.1±2.0
Stormflow	11.0±4.4	3.29±0.54	15.3±1.1	17.9±1.3	0.85±0.02	1.53±0.03	0.59±0.03	0.92±0.01	40.1±0.8	25.1±0.3	20.3±1.0	8.1±0.5	6.4±0.9
ALD													
Seasonal	18.7±4.4	6.59±2.02	13.1±1.1	14.0±1.7	0.94±0.05	1.47±0.05	0.57±0.06	0.88±0.04	40.5±1.5	24.1±1.2	18.8±1.7	8.9±0.7	7.6±2.4
Nival melt	15.9±2.9	4.85±0.93	13.2±0.4	14.4±0.8	0.91±0.02	1.47±0.06	0.54±0.08	0.91±0.02	41.1±1.7	25.0±0.8	18.7±2.2	9.0±0.9	6.1±1.6
Baseflow	20.7±2.3	8.24±0.81	12.4±0.3	12.6±0.5	0.99±0.02	1.45±0.02	0.58±0.02	0.84±0.02	39.8±1.0	23.2±0.6	18.5±0.5	8.9±0.3	9.1±1.6
Stormflow	20.0±8.3	2.84±0.00	14.8±1.7	16.3±1.8	0.91±0.05	1.51±0.03	0.58±0.07	0.91±0.06	41.3±1.3	24.7±1.3	20.0±2.0	8.2±0.8	5.7±1.4
Ptarmigan													
Seasonal	7.9±4.1	3.89±0.73	15.1±1.6	16.3±2.0	0.93±0.07	1.50±0.03	0.57±0.06	0.89±0.04	40.5±1.4	23.2±1.3	20.2±1.4	8.0±0.5	8.0±2.0
Nival melt	7.9±4.2	4.11±0.92	14.4±1.7	15.2±1.4	0.95±0.04	1.48±0.02	0.51±0.06	0.88±0.04	39.7±1.1	24.2±1.4	18.8±0.8	8.3±0.4	8.9±1.8
Baseflow	4.2±1.1	3.76±0.40	15.2±1.4	17.4±2.5	0.88±0.10	1.50±0.02	0.60±0.03	0.89±0.03	40.4±1.5	22.6±0.6	20.5±0.7	8.1±0.2	8.4±2.0
Stormflow	12.3±3.8	3.49±0.25	16.2±1.0	17.1±0.7	0.94±0.04	1.53±0.03	0.61±0.04	0.93±0.01	41.7±0.5	22.7±1.0	21.6±1.1	7.6±0.4	6.4±0.6

Note: ± refers to 1 standard deviation from the mean.

Fig. 5. Seasonal patterns of optical indices: (A) specific UV-absorbance ($SUVA_{254}$), (B) spectral slope in the range of wavelength 275–295 nm (S_{295}), and (C) spectral slope ratio (S_R). The grey area highlights the nival melt in the four streams.

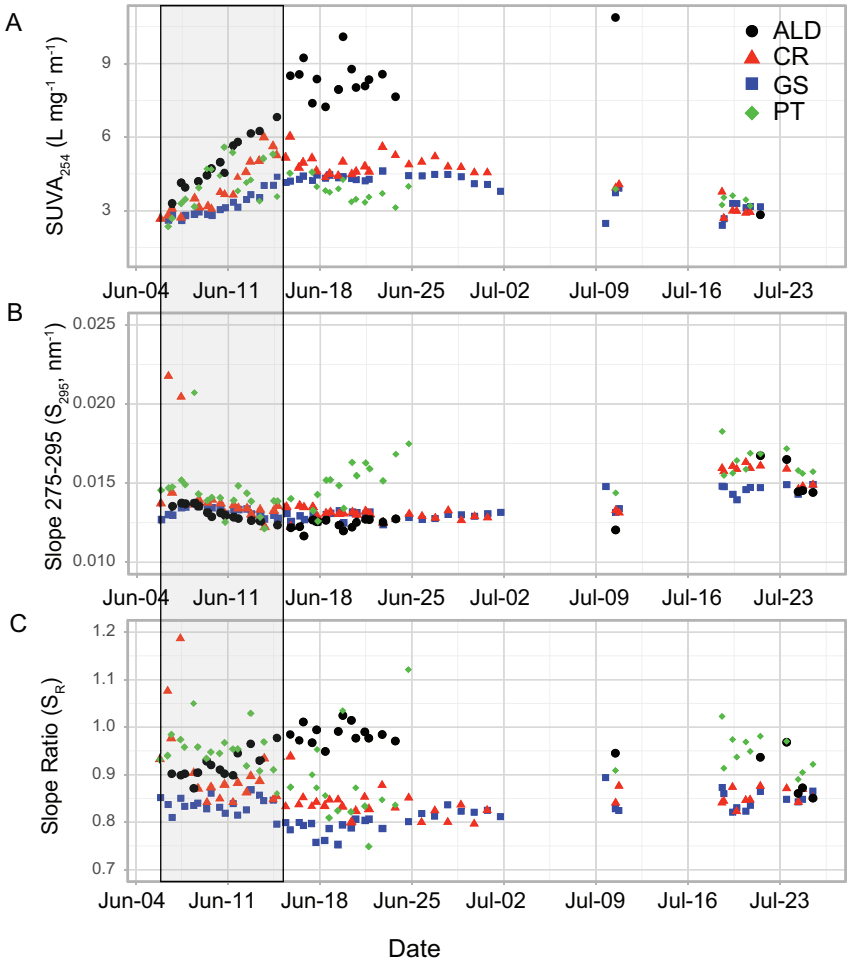

and decreased during the stormflow in undisturbed Goose, in both disturbed catchments Caribou and Ptarmigan, $SUVA_{254}$ values decreased from the onset of the baseflow period (Fig. 5A). Although ALD exhibited high values during baseflow, $SUVA_{254}$ was similar at the end of July in the four catchments (Fig. 5A).

Spectral slopes and S_R have been reported to increase with a decrease of the DOM molecular weight (Helms et al. 2008; Mann et al. 2012). The use of the three indices is relevant because each value may reflect a broad, more complex range of physical and biological processes (Frey et al. 2015). Both S_{295} and S_R values significantly increased with impact of disturbance in the catchments from undisturbed Goose to the most disturbed Ptarmigan (S_{295}: $F = 17.5$, $p < 0.001$; S_{400}: $F = 22.04$, $p < 0.001$; S_R: $F = 47.85$, $p < 0.001$) (Table 3), illustrating a greater export of LMW DOM from disturbed catchments.

Except in ALD, S_{295} and S_R declined during the nival melt until the onset of the baseflow phase and peaked during the stormflow (Figs. 5B and 5C). Thus, Goose, Caribou, and Ptarmigan catchments exported lighter DOM during the onset of the snowmelt and the stormflow period. The DOM weight continuously increased during the nival melt and

streams delivered DOM with a higher molecular weight during the baseflow (i.e. lower spectral slopes and S_R). In the most disturbed Ptarmigan, S_{295} quickly increased from the onset of baseflow reaching high values at the end of June, illustrating the export of an important pool of LMW organic compounds earlier than the moderately disturbed and undisturbed catchments (Fig. 5B). In ALD, S_R followed a trend different from that of S_{295} and was positively correlated with $SUVA_{254}$ ($r = 0.96$, $p < 0.001$) (Figs. 5B and 5C).

Both FI and BIX proved to be good indicators of source of DOM from terrestrial inputs (i.e., plant and soil organic matter, low FI and BIX) to fresh microbially derived organic compounds (i.e., extracellular release and leachate from bacteria and algae, high FI and BIX). Although FI and BIX values highlighted a greater proportion of DOM originated from terrestrial inputs (FI ~1.45 and BIX ~0.55), both mean seasonal FI ($F = 19.09$, $p < 0.001$) and BIX ($F = 17.1$, $p < 0.001$) were significantly higher (fresher and more microbial) in runoff from disturbed catchments than from the undisturbed Goose and particularly in the most disturbed Ptarmigan (Table 3).

During the spring freshet, in the undisturbed Goose, FI was relatively low and changed little, indicating a higher proportion of DOM from terrestrial sources relative to the disturbed catchments, where FI was relatively high, indicating increasing microbial sources (Fig. 6A). The FI decreased relatively rapidly over the first week in ALD and Caribou but remained relatively high (microbial sources) in Ptarmigan (Fig. 6A). For most sites, the BIX was low and increased over the first week of the nival period, indicating increasing freshness the first week. Noteworthy is the highest BIX values in ALD during the onset of spring freshet (~0.65). In the second week of the nival melt, FI and BIX declined in Goose, indicating increasing terrestrial sources and decreasing freshness (Figs. 6A and 6B). In contrast, FI and BIX in the disturbed catchments increased the second week of nival melt, indicating increasing microbial sources and freshness (Figs. 6A and 6B). Both FI and BIX increased during the baseflow and peaked during the stormflow period with similar values in all catchments, indicating fresh and more microbial sources of DOM at the end of the hydrological season (Table 3; Figs. 6A and 6B).

HIX has been proved to be a good proxy of humic substance content or the extent of humification, increasing with a higher degree of humification and microbial processing (Fellman et al. 2010). Seasonal HIX was significantly higher in the undisturbed Goose (0.94) than in the disturbed catchments Caribou, Ptarmigan, and ALD (0.88) ($F = 31.61$, $p < 0.001$) (Table 3), indicating the greater export of humic substances from the undisturbed catchments. During the second stage of the spring freshet, HIX increased in both the undisturbed Goose and the minimally disturbed/less disturbed Caribou, while it declined in the more disturbed and hydrologically connected ALD and Ptarmigan (Fig. 6C). At the end of the spring freshet and during the baseflow, HIX continuously increased in Goose. In Caribou, HIX decreased to values similar to those in Ptarmigan and then remained steady until the end of July (Fig. 6C). In ALD, HIX continuously declined until the first rainfall event when it reached the lowest values (0.77). Thus, during baseflow, the undisturbed Goose exported the most humified DOM (highest HIX) and the moderately disturbed ALD delivered the least humified DOM (Table 3). By the end of stormflow, the four catchments delivered DOM of the same degree of humification (i.e. similar HIX) (Fig. 6C).

PARAFAC modeling

The three aromatic and HMW humic-like components (C1, C2, and C4) explained more than 75% of the total DOM fluorescence in all catchments, with C1 being by far the most predominant component over the seasonal hydrograph (~40%) (Table 3). Both the LMW humic-like component (C3) and the protein-like component (C5) contributions significantly increased with impact of disturbance in the catchments from Goose (Table 3) (C3: $F = 21.73$,

Fig. 6. Seasonal patterns of optical indices: (A) fluorescence index (FI), (B) freshness index (BIX), and (C) humification index (HIX). The grey area highlights the nival melt in the four streams.

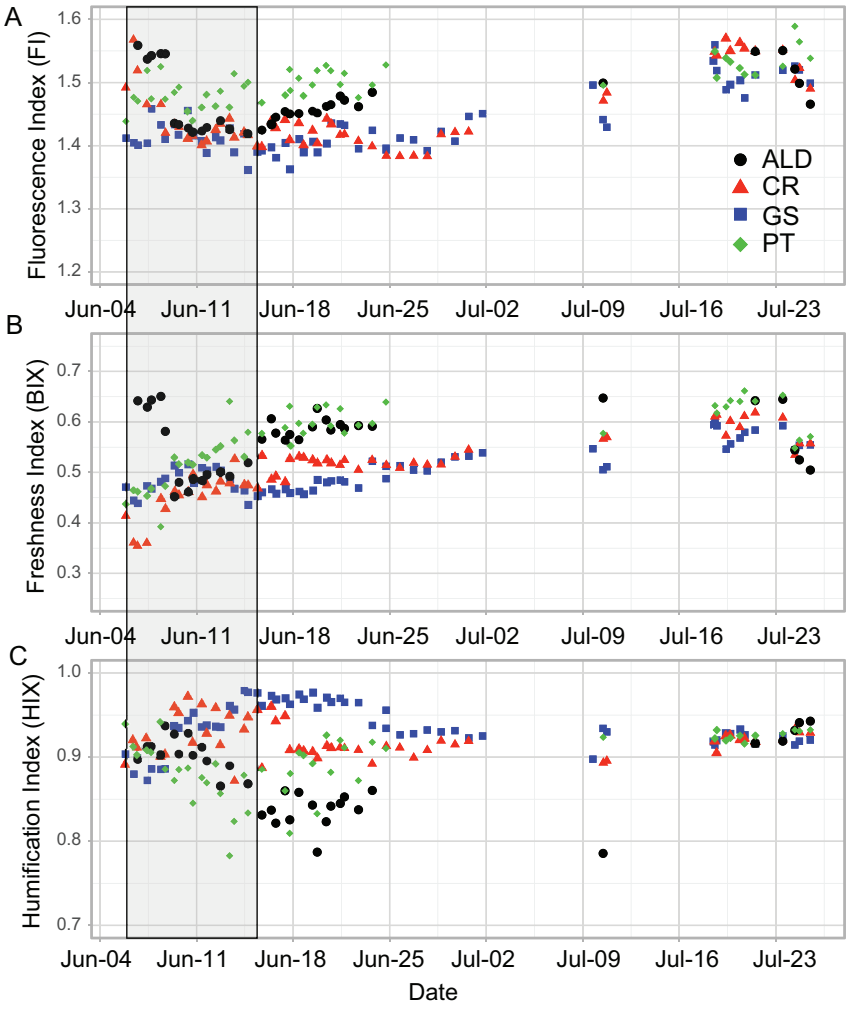

$p < 0.001$; C5: $F = 14.15$, $p < 0.001$). The components C1, C2, and C4 were all positively correlated, with C1 and C4 showing the strongest relationship ($r = 0.70$, $p < 0.001$). Consequently, all of the humic-like components exhibited almost the same seasonal trends, and total contribution of the humic components decreased on average with increasing disturbance impact from the undisturbed Goose to the most disturbed Ptarmigan catchment (Table 3) (Figs. 7A, 7B, and 7D).

During the baseflow and the stormflow periods, the humic-like components were much higher in Goose and Caribou relative to ALD and Ptarmigan (Figs. 7A, 7B, and 7D). Conversely, the LMW humic-like C3 and the protein-like C5 components were higher in the more intensely disturbed Ptarmigan and ALD during baseflow relative to the undisturbed Goose and moderately disturbed Caribou (Figs. 7C and 7E).

All component contributions in Caribou and ALD exhibited patterns and values that were intermediate to the two end-member catchments, the undisturbed Goose and the most disturbed Ptarmigan (Fig. 7). The relative contributions of components in Caribou

Fig. 7. Dissolved organic matter compositional change in the four streams over the discharge period in 2012 illustrating the seasonal pattern of the relative contribution of PARAFAC components to the total fluorescence: (A) component 1, (B) component 2, (C) component 3, (D) component 4, and (E) component 5.

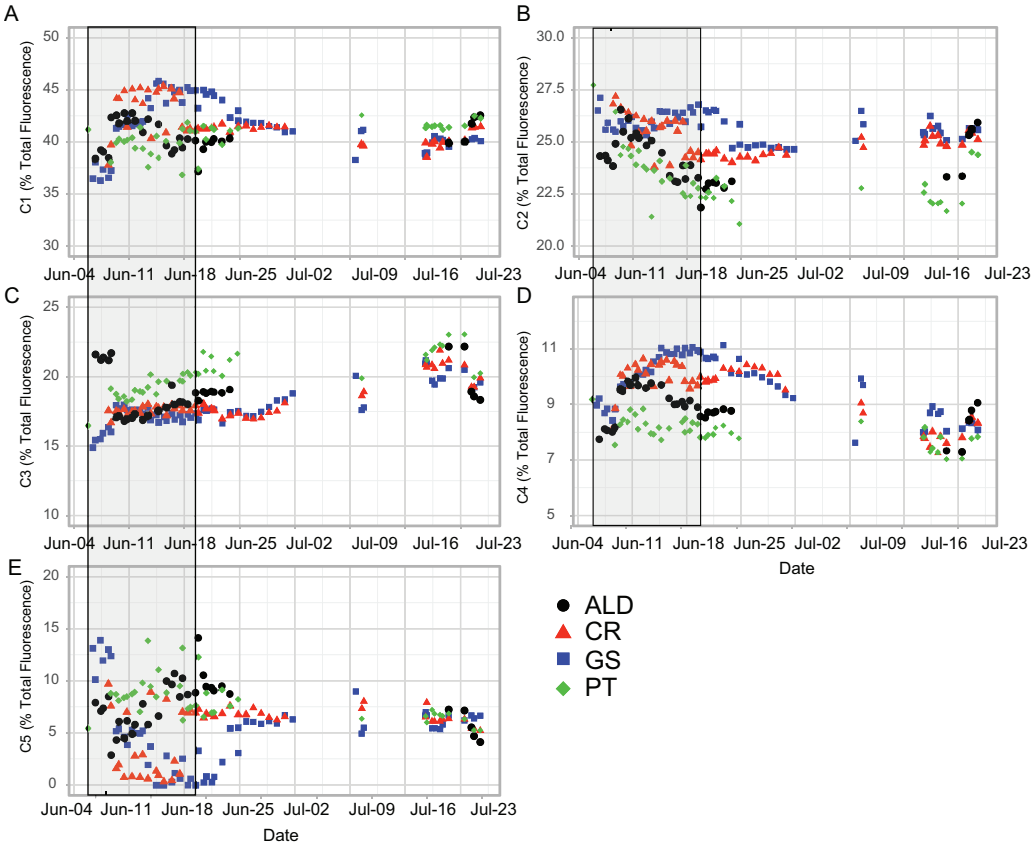

and ALD followed the same trend as in Goose during the nival melt and then trended towards Ptarmigan values at the end of the snowmelt period. Component contributions in ALD, which is more affected by permafrost disturbance relative to Caribou, reached Ptarmigan values earlier than in Caribou. Noteworthy, ALD exhibited high C3 concentrations and low C2 concentrations during the onset of nival melt.

During the nival melt and the baseflow periods, the undisturbed Goose and moderately disturbed Caribou catchments exhibited a higher relative contribution of HMW humic-like components than the most disturbed ALD and Ptarmigan catchments. In Goose and Caribou, C1 and C4 contributions increased during the spring freshet and peaked at the start of the baseflow period. In contrast in ALD and Ptarmigan, C1 and C4 contributions peaked at the end of the first week of the nival melt and continuously decreased until the end of the hydrological season (Figs. 7A, 7B, and 7D).

The most disturbed catchments ALD and Ptarmigan delivered more LMW humic-like C3 and protein-like C5 components than Goose and Caribou during the spring freshet and the baseflow period (Figs. 7C and 7E). Although the most disturbed catchments exhibited a greater proportion of LMW humic-like C3 component, its relative contribution continuously increased during the season in all catchments to reach almost similar values at the end of the stormflow period (Fig. 7C).

In Goose and Caribou, the contribution of the protein-like C5 component declined from almost 15% to 0% during the nival melt and increased during the baseflow period. In disturbed catchments ALD and Ptarmigan, the relative contribution of C5 decreased from the onset of the baseflow period (Fig. 7E). At the end of the stormflow, stream waters from all catchments showed almost similar relative contributions of all components, although C2 was the lowest in Ptarmigan and highest in Goose (Fig. 7).

Relationships between PARAFAC components and optical properties and biogeochemical composition

Unexpectedly, the fluorescence of components and ratios were not correlated with discharge rates (Table 4). Furthermore, no significant correlations between relative contributions of components and DOC, DON, and $SUVA_{254}$ were observed (Table 4). Remarkably, the five components were significantly correlated with NO_3^- content. The three HMW humic-like components (C1, C2, and C4) were negatively correlated with NO_3^- concentration, while C3 and C5 contributions increased with NO_3^- content (Table 4), highlighting their microbial origin.

E350 increased with decreasing contribution of C3 and the increase of the ratio C4:(C4 + C1), suggesting that the contribution of the most HMW and aromatic humic-like component was more predominant in the bulk DOM absorbance than that of the lighter humic-like component (Table 4).

The contributions of all components were strongly related to fluorescence indices (Table 4). The contributions of the three HMW humic-like components (C1, C2, and C4) decreased with FI and BIX, while they increased with HIX (Table 4). Conversely, C3 and C5 relative contributions increased with FI and BIX. The relative contribution of C5 was negatively correlated with HIX, suggesting that the bulk humification degree of DOM decreased with protein-like component production (Table 4). As reported by Cory and McKnight (2005), the C4:(C4 + C1) ratio significantly explained the variation in FI by decreasing with FI increase (Table 4).

The contributions of C2, C4, and C4:(C4 + C1) to the total fluorescence declined with both S_{295} and S_R, highlighting that these components, and C4 in particular, exhibited a HMW. The contributions of C1 and C3:(C3 + C5) were also negatively correlated with S_R, suggesting that C1 exhibited a HMW and that the evolution of the protein-like component may be related to the increased contribution of HMW humic-like components. The contribution of C3 was positively correlated with both spectral slopes and S_R and the contribution of C5 increased with S_R, highlighting that C3 and C5 correspond to light organic compounds.

The contributions to the total fluorescence of C2, C3, and C4 were correlated with TDS, while the protein-like component C5 fluorescence did not display any relationship with TDS (Table 4). The C3 proportion was strongly positively correlated with TDS, while C2 and C4 relative fluorescence and C4:(C4 + C1) were negatively correlated with TDS (Table 4).

Temporal patterns and relationships between optical DOM properties, DOC, DON, DIN, TDS, discharge, and SSC were explored using PCA (Fig. 8). The three first principal components explained 70% of the total variance of the data set. The first principal component corresponds to the shift in molecular weight, freshness, and terrestrial inputs from HMW humic-like PARAFAC components to the LMW humic-like PARAFAC component (C3) associated with inorganic ion concentrations. The second principal component is related to the contribution of the protein-like PARAFAC component (C5) and the decrease in humification. Noteworthy is the positive correlation between SSC and protein-like PARAFAC C5 components (Fig. 8A). DOC, DON, and DIN concentrations and discharge were explained by the third principal component (12.5% of the total variance) (Fig. 8A).

The two first components of the PCA clearly showed that the nival melt, when the DOC fluxes were the highest, and the baseflow resulted in enrichment in humified HMW humic-

Table 4. Pearson's correlation coefficients between relative contribution of PARAFAC components to total fluorescence and discharge (Q), TDS, DOC, TDN, DON, DIN, NO_3^-, and optical indices.

PARAFAC components (%)	Q (mm)	TDS (mg L^{-1})	DOC (mg L^{-1})	TDN (mg L^{-1})	DON (mg L^{-1})	DIN (mg L^{-1})	NO_3^- (mg L^{-1})	FI	BIX	HIX	E350 (m^{-1})	$SUVA_{254}$ (L mg^{-1} C m^{-1})	S_{295} (nm^{-1})	S_{400} (nm^{-1})	S_R
C1	−0.33	−0.08	−0.21	−0.12	−0.06	**−0.14***	**−0.37****	**−0.47****	**−0.49****	**0.76****	−0.17	−0.03	−0.13	0.16	**−0.41****
C2	0.26	**−0.37****	0.40	0.06	0.19	**−0.21***	**−0.46****	**−0.51****	**−0.82****	**0.64****	0.23	−0.33	**−0.32****	0.14	**−0.60****
C3	−0.29	**0.65****	0.00	**0.34****	0.23	**0.32****	**0.50****	**0.90****	**0.88****	−0.14	**−0.26***	−0.17	**0.73****	**0.37****	**0.29***
C4	−0.09	**−0.54****	−0.07	**−0.25****	−0.10	**−0.36****	**−0.56****	**−0.88****	**−0.80****	**0.55****	0.16	0.12	**−0.62****	−0.16	**−0.48****
C5	0.28	0.05	−0.02	−0.05	−0.13	0.13	**0.29****	**0.34****	**0.49****	**−0.88****	0.09	0.21	0.04	−0.3	**0.53****
C4:(C4 + C1)	0.10	**−0.68****	0.05	**−0.27****	−0.09	**−0.40****	**−0.55****	**−0.91****	**−0.78****	**0.25***	**0.34***	0.19	**−0.77****	−0.33	**−0.38****
C3:(C3 + C5)	−0.31	0.00	−0.02	0.06	0.13	−0.11	**−0.21****	**−0.27****	**−0.40****	**0.85****	−0.14	−0.21	0.01	0.33	**−0.50****

Note: *Correlations significant at $p < 0.05$; **correlations significant at $p < 0.01$. Bolds values represent all significant correlation coefficients.

Fig. 8. Graphical representation of principal component analysis of the PARAFAC relative contribution of components, optical indices, suspended sediment concentration (SSC), discharge (Q), TDS, DOC, DON, and DIN. (A) Explanatory variable loadings are shown as arrows and their colour represents their respective contributions. (B) Scores across the first and second principal components for all samples labeled by sites and hydrological periods. (C) Scores across the first and second principal components for all samples labeled by sites and DOC fluxes.

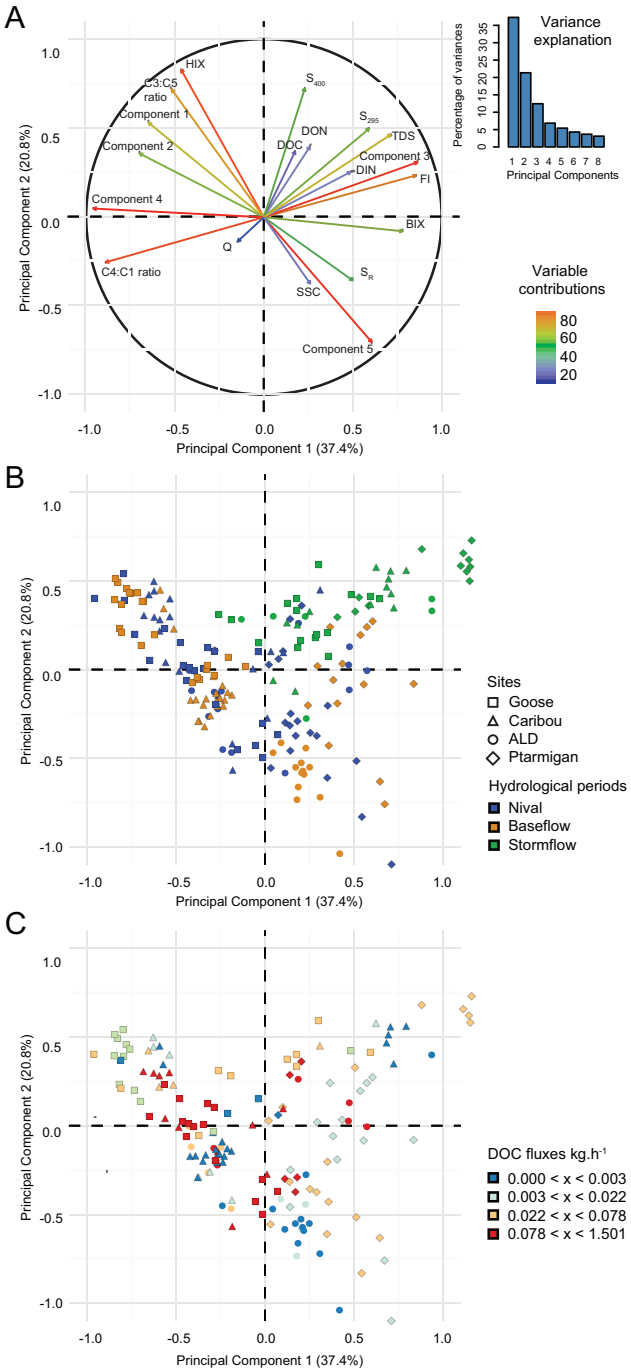

like components (C1, C2, and C4) and high contribution of protein-like components (C5) in disturbed catchments (Figs. 8B and 8C). The stormflow, which significantly contributed to DOM yield during the season from all catchments (Fig. 8C), exhibited a shift in composition with enrichment in fresh LMW humic-like components (C3) associated with high concentrations in organic and inorganic solute concentrations (Fig. 8B).

Discussion

As observed in other Arctic watersheds, all studied streams experienced strong seasonality in discharge, with most of the flow occurring during the quick spring freshet. Streams from headwater catchments exhibit higher concentrations of DOM than main stems in large Arctic watersheds (Spencer et al. 2008; Wickland et al. 2012; Mann et al. 2015) due to large inputs from terrestrial DOM leaching and mobilization of ancient DOC from permafrost thaw (Mann et al. 2015; Spencer et al. 2015). Recent studies have shown that most of the old-permafrost DOM mobilized in small streams is degraded through microbial activity and photodegradation within soils and the fluvial system (Drake et al. 2015; Mann et al. 2015; Spencer et al. 2015).

Due to significant changes expected in the Arctic, the quantification and the characterization of the DOM exported from both small and large catchments is a growing concern. Despite this rising interest, a lack of consensus remains about the consequences of permafrost degradation on the potential biodegradability of the DOM in Arctic rivers. Only a few studies have been performed in Arctic headwater catchments (Wickland et al. 2012; Larouche et al. 2015), and to our knowledge, this study is the first conducted in the High Arctic region.

The characterization of permafrost-derived DOM in headwater catchments is challenging because of the strong seasonality in discharge, the related rapid DOM evolution, and the heterogeneity of Arctic landscapes (Wickland et al. 2012; Drake et al. 2015). In this study, we examine high-frequency sampling of DOM composition aiming to capture evolution of exported DOM from headwater catchments affected by permafrost disturbance in the High Arctic.

Linking optical properties to DOM composition

The PARAFAC components in undisturbed and disturbed catchments in CBAWO were identical to components previously identified in surface waters and Arctic streams (Cory and McKnight 2005; Fellman et al. 2010; Cory and Kaplan 2012; Mann et al. 2016).

Component C1, which displayed the highest relative contribution to the total fluorescence, has been associated with terrestrially derived material such as lignin compounds, lignin breakdown products, or degraded lignin having high aromatic carbon content (Cory and McKnight 2005; Fellman et al. 2010; Cory and Kaplan 2012). C2 is associated with the product of lignin breakdown and syringaldehyde content (Cory and McKnight 2005; Fellman et al. 2010; Cory and Kaplan 2012). The spectral characteristics of C4 suggest that it is a partially or fully reduced semiquinone from higher plant material with a high aromatic carbon content as described in Cory and McKnight (2005) and in Cory and Kaplan (2012). Our study also found that the ratio C4:(C4 + C1) was strongly inversely correlated with FI, highlighting the higher-plant origin and high aromatic carbon content of C4 and the likely microbial processing of C1 (Cory and McKnight 2005).

Component C3, which was identified as a UVA humic-like acid displaying a LMW, is likely associated with the aliphatic carbon content (Cory and Kaplan 2012; Vonk et al. 2013*a*; Mann et al. 2016). C5 represents the tryptophan-like components (Fellman et al. 2010; Cory and Kaplan 2012; Mann et al. 2016). No tyrosine-like components were observed in this study. Both the LMW humic-like (C3) and the protein-like components (C5) are ubiquitous and originate from terrestrial and marine precursors and autochthonous activity.

The predominance of terrestrial inputs in DOM has also been shown in CBAWO in the main river streams and riverine sediments (Woods et al. 2011; Grewer et al. 2015). Woods et al. (2011) highlighted that plant-derived organic matter originated from primarily non-woody angiosprem vegetation and reported that CBAWO streams exhibited average lignin-derived phenol content relative to total DOC much lower than typical freshwater, with values close to those from heavily glaciated Arctic watersheds.

Linking DOM composition to its potential biodegradability

In both soils and rivers, heterotrophic bacteria mineralize both terrestrially derived and microbially derived DOM for energy and growth. Lability (i.e., biodegradabiliy) of DOM refers to its biological availability for uptake and mineralization by microorganisms (Schmidt et al. 2011; Cory and Kaplan 2012; Abbott et al. 2014; Larouche et al. 2015). Because DOM is a complex mixture of organic molecules, the assessment of the DOM lability in rivers is challenging and it is difficult to connect the molecular signatures or classes of organic compounds to their respective turnover time (Cory and Kaplan 2012; Marin-Spiotta et al. 2014). Moreover, recent studies highlight that biotic and abiotic environmental factors (e.g., temperature, oxygen availability, vegetation, background microbial activity) can be more important controls on organic matter turnover rates than the molecular structure (Schmidt et al. 2011; Marin-Spiotta et al. 2014). The only direct way to assess the biodegradability of DOM is through incubation experiments. Because they are time consuming, proxies using DOM composition such as absorbance/fluorescence spectroscopy are relevant for high-temporal resolution studies (Cory and Kaplan 2012). Differences in experimental approaches, the seasonal variability along the fluvial network, and the high heterogeneity in landscapes contribute to the current lack of consensus about the lability of DOM exported from Arctic rivers and its likely evolution with climate change (Frey and McClelland 2009;Wickland et al. 2012; Larouche et al. 2015).

Considering that environmental factors mediate the influence of the molecular structure on the biodegradability of DOM (Schmidt et al. 2011; Marin-Spiotta et al. 2014), our study investigated the composition of DOM exported from catchments showing similar climate, vegetation, substrate, and landscape properties. Thus, the similar biome conditions allowed us to assess changes in the potential lability of DOM through the evolution of both the DOM composition (Fellman et al. 2008; Balcarczyk et al. 2009; Vonk et al. 2013*a*) and the inorganic nitrogen concentrations (Holmes et al. 2008; Wickland et al. 2012; Abbott et al. 2014).

Many studies have shown that the DOM exported during the spring freshet by Arctic rivers was highly labile (Raymond et al. 2007; Holmes et al. 2008; Spencer et al. 2008; Mann et al. 2012) despite being primarily derived from plant biomass and soil organic matter. This terrestrially derived DOM is young and displays a high proportion of HMW humic acid, which was previously considered as recalcitrant (Mann et al. 2012). The DOM exported during the recession period progressively became more refractory (Holmes et al. 2008; Mann et al. 2012; Wickland et al. 2012). Because of the positive correlation between DOM biodegradability and DIN, these studies suggested that DOM lability was related to high concentrations of inorganic nitrogen stimulating DOM mineralization and conversely the low nitrogen content limiting the DOM lability (Holmes et al. 2008; Mann et al. 2012; Wickland et al. 2012). Abbott et al. (2014) also showed that the DOM biodegradability increased with the initial nutrient concentration and the nutrient addition in incubations increased more the DOM biodegradability in samples with higher initial nutrient concentrations.

Although the relationship between DOM lability and composition varies between environments, for given environmental conditions, many studies associated specific PARAFAC components and fluorescence indices with DOM lability in Arctic environments.

Thus, we interpret that UVC humic-like components (C1 and C2) that display HMW and higher degree of aromaticity are likely recalcitrant (Fellman et al. 2008; Balcarczyk et al. 2009; Vonk et al. 2013*a*). Conversely, protein-like fluorescence has been associated with an increase of DOM biodegradability (Amon et al. 2001; Cammack et al. 2004; Fellman et al. 2008; Balcarczyk et al. 2009). According to many studies, tryptophan-like fluorescence, which represents relative recent and unaltered amino acids and less-degraded peptide material compared to tyrosine, was a good predictor of DOC lability (Fellman et al. 2008; Balcarczyk et al. 2009; Wickland et al. 2012). In contrast, Cory and Kaplan (2012) showed that only 27% of tryptophan-like components were labile or semi-labile, while all tyrosine-like DOM was labile. Furthermore, other studies have shown LMW humic acids and FI to be good predictors of increasing DOM lability (Wickland et al. 2012; Vonk et al. 2013*b*; Drake et al. 2015).

Based on all of these studies and considering similar environmental factors (i.e., vegetation, climate, landscape, oxygen availability) between catchments, we interpret that the potential biodegradability of the DOM exported likely increases with an increase in inorganic nitrogen concentrations and an increase in the contribution of the LMW humic-like and protein-like components. The inorganic nitrogen forms and the light organic components are both consumed and produced by microorganisms, and their increases reflect and support greater microbial activity.

DOM concentration and composition evolution during the hydrologic season

As expected in Arctic catchments, DOC concentrations peaked during the onset of nival melt leading to an export ranging from 76% in Ptarmigan to 99% in ALD of the total DOM delivered during the spring freshet. High DOC and DON concentrations are evidence of the large pool of DOM already available and mobilized with the snowmelt, and decreasing concentrations during the nival melt are due to the dilution with increasing discharge and depletion of the pool. The elevated DOM fluxes generated by rainfall events in July resulted from an increase of the pool of available terrestrial DOM in the shallow soils. The strong seasonality of DOM fluxes was associated with changes in DOM composition, which varied between the undisturbed and the disturbed catchments.

In the undisturbed Goose catchment, the onset of nival melt resulted in an increase in the contribution of HMW humic-like DOM. The lower DOM freshness and the increase of molecular weight and aromaticity illustrate an increase in terrestrial inputs from plant-derived compounds and humified organic matter from the shallow organic soil layers in the catchment (Holmes et al. 2008; Balcarczyk et al. 2009; Mann et al. 2012). Runoff was constrained to surface layers due to the impermeability of the frozen ground. A shift in DOM composition occurred during the baseflow with an increase in the contribution of protein-like and less aromatic humic-like components. This shift illustrates the enhancement of autochthonous activity and the increased production of fresh microbially derived DOM in the soil and the river. Baseflow and stormflow conditions were characterized by declines in molecular weight and aromaticity. This DOM composition shift was previously observed in CBAWO by Woods et al. (2011), who showed that the degraded lignin-derived phenols displayed a decreasing degree of oxidation throughout the hydrologic season. The authors suggested that the oxidation decrease over the spring flush may result from the melting water percolated deeper into the soil providing fresher organic compounds (Woods et al. 2011).

In Ptarmigan, the decline in FI during the first days illustrated the storage of fresh DOM in the snowpack in disturbed catchments. Louiseize et al. (2014) showed that a high proportion of NO_3^- in Ptarmigan originated from nitrification in the snowpack and soil surface. All catchments experienced similar trends during the onset of the spring freshet. However, from the second week onwards, while the contribution of HMW humic-like components still increased in the undisturbed catchment, in the disturbed catchments, the relative

contribution of humified HMW humic-like components declined and the contribution of fresh LMW humic-like and protein components rose. The decrease in HMW humic-like components illustrates that the depletion of the surface DOM pool may occur earlier in the disturbed catchments than in the undisturbed catchments due to reduced vegetation cover resulting from the ALDs. The simultaneous increase in LMW humic-like and protein-like components illustrates both an increase in microbial activity within soils and rivers as previously suggested (Woods et al. 2011; Louiseize et al. 2014) and a greater pool of microbially derived DOM in soils near disturbances as demonstrated by Pautler et al. (2010).

The contribution of the LMW humic-like component, associated with less aromatic and more microbially derived DOM, peaked during the stormflow period and was correlated with the increase in inorganic solute concentrations. The increase in TDS and the DOM composition shift are clear indicators of change in flow path from surface to subsurface runoff deeper in the active layer on the permafrost table (Striegl et al. 2005; Neff et al. 2006; Spencer et al. 2008). Deeper flow provides inorganic ions and likely transports more hydrophilic DOM previously stored at depth. A longer residence time in the active layer results in changes in DOM composition due to the increase of microbial processing of the biodegradable DOM pool and the selective sorption of hydrophobic compounds in the mineral soil leaving hydrophilic compounds in solution (Kalbitz et al. 2000; Balcarczyk et al. 2009). Thus, DOM released from the catchment late in the season may therefore be enriched in more hydrophilic compounds that were not mineralized as CO_2 within the active layer and release to the atmosphere (Balcarczyk et al. 2009; Drake et al. 2015). A decrease in DOC concentration associated with an enrichment in hydrophilic organic compounds illustrates an increasing subsurface discharge (O'Donnell et al. 2012).

Disturbance impact on DOM composition

As observed in other studies, the ALDs in disturbed catchments caused the strong decline in DOM export (Balcarczyk et al. 2009; Larouche et al. 2015). The stream in Ptarmigan drains in a well-incised channel through two elongated disturbances composed of mineral soils connected to downstream. The disturbances disrupted and transported the organic layers downslope (Lamoureux and Lafrenière 2009). The smaller pool of DOM from removal of organic-rich surface layers and the lower soil organic carbon content at depth (Grewer et al. 2016) decreased the terrestrial DOM inputs from surface runoff in disturbed catchments. As previously observed in CBAWO, streams from disturbed catchments exhibited higher concentrations of nitrate and inorganic solutes (Lafrenière and Lamoureux 2013; Louiseize et al. 2014).

The undisturbed catchment exported a higher proportion of terrestrial HMW humic-like components from plant-derived materials and soil organic matter, consistent with the predominance of HMW lipids and minor fraction of short-chain *n*-alkanes and *n*-alkanols shown by Grewer et al. (2015). Conversely, the contributions of less-humified and light protein-like components increased with disturbance magnitude, illustrating a greater microbial activity in disturbed catchments. Previous studies in CBAWO have found enhancement of microbial activity and degradation of soil organic matter in both soils near ALDs and streams (Pautler et al. 2010; Louiseize et al. 2014). However, the authors suggested that the rise in microbial activity may lead to the degradation and depletion of labile soil organic matter and the microbial substrate limitation in soils within the disturbed catchments (Pautler et al. 2010). The clay-rich scar zones of the ALDs restricted the vertical water flow and channelized the flow downslope through surficial mineral soils leading to higher nitrification rates and NO_3^- export to streams (Louiseize et al. 2014). The NO_3^- input likely supported the rise in microbial activity during the years after the disturbance was active.

The increased contribution of the LMW humic-like component in disturbed catchments while the contribution of protein-like components declined during the stormflow indicates that the DOM was likely derived from deep soil layers previously inaccessible to surface runoff. The runoff through the new surficial mineral layers and deep layers (associated with higher concentrations of dissolved solutes (Lafrenière and Lamoureux 2013)) was likely a source of DOM, which was previously stored in the permafrost. Our results agree with the evidence of less-degraded DOM possibly preserved within permafrost soils prior to the ALD disturbance as observed in sediments from disturbed catchments (Grewer et al. 2015). Grewer et al. (2015) also showed that permafrost-derived organic matter is characterized by a lower degree of alteration in acyclic aliphatic lipids, which is consistent with the observed rise of the C3 contribution in Ptarmigan in this study.

The combination of higher concentrations of inorganic nitrogen and the greater proportion of LMW humic acids may lead to a relative increase of the potential lability of DOM exported from High Arctic headwater catchments affected by permafrost degradation (Abbott et al. 2014). The shift in DOM composition and potential lability is still evident 4 years after the disturbances occurred.

Conclusion

This study reports on the seasonal evolution of DOM composition in water streams from an undisturbed catchment (Goose) and three catchments (Caribou, ALD, and Ptarmigan) that were subject to increasing degrees of disturbance in a High Arctic watershed. We demonstrate that DOM characterization using optical and chemical analyses provides reliable information on the evolution in source of DOM and the relative changes in its biodegradability with seasonal evolution of thaw and varying degrees of disturbance.

The DOM export throughout the hydrologic season decreased with the disturbance magnitude. The undisturbed Goose catchment exhibited higher DOM concentrations and a greater discharge than in disturbed Caribou, ALD, and Ptarmigan catchments likely due to a great pool of organic matter in surface layers and a sustained discharge by snowmelt from snowpacks located in channels and depressions. Although in all streams, the exported DOM mostly originated from terrestrial inputs, catchments with increasing degree of disturbance delivered fresher, lighter, and less-humified DOM and experienced an enhancement of the autochthonous microbial activity. The LMW humic-like component enrichment in disturbed catchments likely originated from both the enhancement of microbial activity with higher microbial NO_3^- content and the export of less-decomposed DOM previously stored in permafrost mineral layers.

While the bulk DOM lability was likely at maxima in the undisturbed Goose catchment during the nival melt, higher concentrations of LMW humic acids and amino acids, combined with a greater DIN availability during the stormflow, will likely lead to the export of a greater proportion of labile DOM by High Arctic disturbed catchments along the entire hydrologic season. Furthermore, the modification in hydrological regime from a nival to pluvial system will likely change the composition and the potential biodegradability of DOM exported from both disturbed and undisturbed headwater catchments.

Acknowledgements

This research was funded by the ArcticNet Network of Centres of Excellence of Canada, the Natural Sciences and Engineering Research Council of Canada (NSERC) Discovery Frontiers ADAPT, and individual discovery grants. Logistics support was provided by the Polar Continental Shelf Programme. We also gratefully acknowledge the 2007 and 2012 CBAWO

field research teams. We also thank the two anonymous reviewers for their great comments leading to improvements of the paper.

References

Abbott, B.W., Larouche, J.R., Jones, J.B., Bowden, W.B., and Balser, A.W. 2014. Elevated dissolved organic carbon biodegradability from thawing and collapsing permafrost. J. Geophys. Res. **119**(10): 2049–2063. doi: 10.1002/2014JG002678.

Amon, R.M.W., Fitznar, H.-P., and Benner, R. 2001. Linkages among the bioreactivity, chemical composition, and diagenetic state of marine dissolved organic matter. Limnol. Oceanogr. **46**(2): 287–297. doi: 10.4319/lo.2001.46.2.0287.

Atkinson, D.M., and Treitz, P. 2012. Arctic ecological classifications derived from vegetation community and satellite spectral data. Rem. Sens. **4**(12): 3948–3971. doi: 10.3390/rs4123948.

Balcarczyk, K.L., Jeremy, B.J.J., Jaffé, R., and Maie, N. 2009. Stream dissolved organic matter bioavailability and composition in watersheds underlain with discontinuous permafrost. Biogeochemistry. **94**(3): 255–270. doi: 10.1007/s10533-009-9324-x.

Cammack, W.L., Kalff, J., Prairie, Y.T., and Smith, E.M. 2004. Fluorescent dissolved organic matter in lakes: relationships with heterotrophic metabolism. Limnol. Oceanogr. **49**(6): 2034–2045. doi: 10.4319/lo.2004.49.6.2034.

Cockburn, J.M.H., and Lamoureux, S.F. 2008. Hydroclimate controls over seasonal sediment yield in two adjacent High Arctic watersheds. Hydrol. Process. **22**(12): 2013–2027. doi: 10.1002/hyp.6798.

Cory, R.M., and Kaplan, L.A. 2012. Biological lability of streamwater fluorescent dissolved organic matter. Limnol. Oceanogr. **57**(5): 1347–1360. doi: 10.4319/lo.2012.57.5.1347.

Cory, R.M., and McKnight, D.M. 2005. Fluorescence spectroscopy reveals ubiquitous presence of oxidized and reduced quinones in dissolved organic matter. Environ. Sci. Technol. **39**(21): 8142–8149. doi: 10.1021/es0506962.

Cory, R.M., Miller, M.P., McKnight, D.M., Guerard, J.J., and Miller, P.L. 2010. Effect of instrument-specific response on the analysis of fulvic acid fluorescence spectra. Limnol. Oceanogr. **8**(2): 67, doi: 10.4319/lom.2010.8.67.

Drake, T.W., Wickland, K.P., Spencer, R.G.M., McKnight, D.M., and Striegl, R.G. 2015. Ancient low-molecular-weight organic acids in permafrost fuel rapid carbon dioxide production upon thaw. Proc. Natl Acad. Sci. U.S.A. **112**(45): 13946–13951. doi: 10.1073/pnas.1511705112.

Environment Canada. 2009. National Climate Data and Information Archive, Mould Bay, NWT. http://climate.weatheroffice.gc.ca/.

Fellman, J.B., D'Amore, D.V., Hood, E., and Boone, R.D. 2008. Fluorescence characteristics and biodegradability of dissolved organic matter in forest and wetland soils from coastal temperate watersheds in southeast Alaska. Biogeochemistry. **88**(2): 169–184. doi: 10.1007/s10533-008-9203-x.

Fellman, J.B., Hood, E., and Spencer, R.G. 2010. Fluorescence spectroscopy opens new windows into dissolved organic matter dynamics in freshwater ecosystems: a review. Limnol. Oceanogr. **55**(6): 2452–2462. doi: 10.4319/lo.2010.55.6.2452.

Finlay, J., Neff, J., Zimov, S., Davydova, A., and Davydov, S. 2006. Snowmelt dominance of dissolved organic carbon in high-latitude watersheds: implications for characterization and flux of river DOC. Geophys. Res. Lett. **33**(10): L10401, doi: 10.1029/2006GL025754.

French, H.M. 2007. The periglacial environment. 3rd ed. Wiley.

Frey, K.E., and McClelland, J.W. 2009. Impacts of permafrost degradation on Arctic river biogeochemistry. Hydrol. Process. **23**(1): 169–182. doi: 10.1002/hyp.7196.

Frey, K.E., Sobczak, W.V., Mann, P.J., and Holmes, R.M. 2015. Optical properties and bioavailability of dissolved organic matter along a flow-path continuum from soil pore waters to the Kolyma River, Siberia. Biogeosci. Discuss. **12**(15): 12321–12347. doi: 10.5194/bgd-12-12321-2015.

Grewer, D.M., Lafrenière, M.J., Lamoureux, S.F., and Simpson, M.J. 2015. Potential shifts in Canadian High Arctic sedimentary organic matter composition with permafrost active layer detachments. Org. Geochem. **79**: 1–13. doi: 10.1016/j.orggeochem.2014.11.007.

Grewer, D.M., Lafrenière, M.J., Lamoureux, S.F., and Simpson, M.J. 2016. Redistribution of soil organic matter by permafrost disturbance in the Canadian High Arctic. Biogeochemistry. **128**: 397–415. doi: 10.1007/s10533-016-0215-7.

Guido, G., Scott, G., McGuire, A.D., Vladimir, E.R., and Edward, A.G.S. 2016. Changing permafrost in a warming world and feedbacks to the Earth system. Environ. Res. Lett. **11**(4): 040201, doi: 10.1088/1748-9326/11/4/040201.

Helms, J.R., Stubbins, A., Ritchie, J.D., Minor, E.C., Kieber, D.J., and Mopper, K. 2008. Absorption spectral slopes and slope ratios as indicators of molecular weight, source, and photobleaching of chromophoric dissolved organic matter. Limnol. Oceanogr. **53**(3): 955–969. doi: 10.4319/lo.2008.53.3.0955.

Hernes, P.J., and Benner, R. 2006. Terrigenous organic matter sources and reactivity in the North Atlantic Ocean and a comparison to the Arctic and Pacific oceans. Mar. Chem. **100**(1–2): 66–79. doi: 10.1016/j.marchem.2005.11.003.

Hodgson, D.A., and Vincent, J.-S. 1984. A 10,000 yr B.P. extensive ice shelf over Viscount Melville Sound, Arctic Canada. Quaternary Res. **22**(1): 18–30. doi: 10.1016/0033-5894(84)90003-6.

Holmes, R.M., McClelland, J.W., Raymond, P.A., Frazer, B.B., Peterson, B.J., and Stieglitz, M. 2008. Lability of DOC transported by Alaskan rivers to the Arctic Ocean. Geophys. Res. Lett. **35**(3): L03402, doi: 10.1029/2007GL032837.

Hu, C., Muller-Karger, F.E., and Zepp, R.G. 2002. Absorbance, absorption coefficient, and apparent quantum yield: a comment on common ambiguity in the use of these optical concepts. Limnol. Oceanogr. **47**(4): 1261–1267. doi: 10.4319/lo.2002.47.4.1261.

Hugelius, G., Strauss, J., Zubrzycki, S., Harden, J.W., Schuur, E.A.G., Ping, C.L., Schirrmeister, L., Grosse, G., Michaelson, G.J., et al. 2014. Estimated stocks of circumpolar permafrost carbon with quantified uncertainty ranges and identified data gaps. Biogeosciences. **11**(23): 6573–6593. doi: 10.5194/bg-11-6573-2014.

IPCC. 2013. Climate change 2013: the physical science basis. Contribution of Working Group I to the Fifth Assessment Report of the Intergovernmental Panel on Climate Change. Cambridge University Press, Cambridge, UK.

Kalbitz, K., Solinger, S., Park, J.H., Michalzik, B., and Matzner, E. 2000. Controls on the dynamics of dissolved organic matter in soils: a review. Soil Sci. **165**(4): 277–304. doi: 10.1097/00010694-200004000-00001.

Kawahigashi, M., Kaiser, K., Kalbitz, K., Rodionov, A., and Guggenberger, G. 2004. Dissolved organic matter in small streams along a gradient from discontinuous to continuous permafrost. Glob. Change Biol. **10**(9): 1576–1586. doi: 10.1111/j.1365-2486.2004.00827.x.

Kawahigashi, M., Kaiser, K., Rodionov, A., and Guggenberger, G. 2006. Sorption of dissolved organic matter by mineral soils of the Siberian forest tundra. Glob. Change Biol. **12**(10): 1868–1877. doi: 10.1111/j.1365-2486.2006.01203.x.

Lafrenière, M.J., and Lamoureux, S.F. 2013. Thermal perturbation and rainfall runoff have greater impact on seasonal solute loads than physical disturbance of the active layer. Permafrost Periglacial Process. **24**(3): 241–251. doi: 10.1002/ppp.1784.

Lafrenière, M.J., Laurin, E., and Lamoureux, S.F. 2013. The impact of snow accumulation on the active layer thermal regime in high Arctic soils. Vadose Zone J. **12**(1): vzj2012.0058

Lamoureux, S.F., and Lafrenière, M.J. 2009. Fluvial impact of extensive active layer detachments, Cape Bounty, Melville Island, Canada. Arct. Antarct. Alp. Res. **41**(1): 59–68. doi: 10.1657/1523-0430-41.1.59.

Lamoureux, S.F., Lafrenière, M.J., and Favaro, E.A. 2014. Erosion dynamics following localized permafrost slope disturbances. Geophys. Res. Lett. **41**(15): 5499–5505. doi: 10.1002/2014GL060677.

Larouche, J.R., Abbott, B.W., Bowden, W.B., and Jones, J.B. 2015. The role of watershed characteristics, permafrost thaw, and wildfire on dissolved organic carbon biodegradability and water chemistry in Arctic headwater streams. Biogeosci. Discuss. **12**(5): 4021–4056. doi: 10.5194/bgd-12-4021-2015.

Laurion, I., and Mladenov, N. 2013. Dissolved organic matter photolysis in Canadian arctic thaw ponds. Environ. Res. Lett. **8**(3): 035026, doi: 10.1088/1748-9326/8/3/035026.

Lewis, T., Lafrenière, M.J., and Lamoureux, S.F. 2012. Hydrochemical and sedimentary responses of paired High Arctic watersheds to unusual climate and permafrost disturbance, Cape Bounty, Melville Island, Canada. Hydrol. Process. **26**(13): 2003–2018. doi: 10.1002/hyp.8335.

Lewkowicz, A.G. 2007. Dynamics of active-layer detachment failures, Fosheim Peninsula, Ellesmere Island, Nunavut, Canada. Permafrost Periglacial Process. **18**(1): 89–103. doi: 10.1002/ppp.578.

Louiseize, N.L., Lafrenière, M.J., and Hastings, M.G. 2014. Stable isotopic evidence of enhanced export of microbially derived NO_3^- following active layer slope disturbance in the Canadian High Arctic. Biogeochemistry. **121**(3): 565–580. doi: 10.1007/s10533-014-0023-x.

Mann, P.J., Davydova, A., Zimov, N., Spencer, R.G.M., Davydov, S., Bulygina, E., Zimov, S., and Holmes, R.M. 2012. Controls on the composition and lability of dissolved organic matter in Siberia's Kolyma River basin. J. Geophys. Res. **117**(G1): G01028, doi: 10.1029/2011JG001798.

Mann, P.J., Eglinton, T.I., McIntyre, C.P., Zimov, N., Davydova, A., Vonk, J.E., Holmes, R.M., and Spencer, R.G.M. 2015. Utilization of ancient permafrost carbon in headwaters of Arctic fluvial networks. Nat. Commun. **6**: 7856, doi: 10.1038/ncomms8856.

Mann, P., Spencer, R., Hernes, P., Six, J., Aiken, G., Tank, S., McClelland, J., Butler, K., Dyda, R., and Holmes, R. 2016. Pan-Arctic trends in terrestrial dissolved organic matter from optical measurements. Front. Earth Sci. **4**: 25, doi: 10.3389/feart.2016.00025.

Marin-Spiotta, E., Gruley, K.E., Crawford, J., Atkinson, E.E., Miesel, J.R., Greene, S., Cardona-Correa, C., and Spencer, R.G.M. 2014. Paradigm shifts in soil organic matter research affect interpretations of aquatic carbon cycling: transcending disciplinary and ecosystem boundaries. Biogeochemistry. **117**(2–3): 279–297. doi: 10.1007/s10533-013-9949-7.

McKnight, D.M., Boyer, E.W., Westerhoff, P.K., Doran, P.T., Kulbe, T., and Andersen, D.T. 2001. Spectrofluorometric characterization of dissolved organic matter for indication of precursor organic material and aromaticity. Limnol. Oceanogr. **46**(1): 38–48. doi: 10.4319/lo.2001.46.1.0038.

McNamara, J.P., Kane, D.L., Hobbie, J.E., and Kling, G.W. 2008. Hydrologic and biogeochemical controls on the spatial and temporal patterns of nitrogen and phosphorus in the Kuparul River, Arctic Alaska. Hydrol. Process. **22**(17): 3294–3309. doi: 10.1002/hyp.6920.

Murphy, K.R., Stedmon, C.A., Waite, T.D., and Ruiz, G.M. 2008. Distinguishing between terrestrial and autochthonous organic matter sources in marine environments using fluorescence spectroscopy. Mar. Chem. **108**(12): 40–58. doi: 10.1016/j.marchem.2007.10.003.

Murphy, K.R., Stedmon, C.A., Graeber, D., and Bro, R. 2013. Fluorescence spectroscopy and multi-way techniques. PARAFAC. Anal. Methods. **5**(23): 6557–6566. doi: 10.1039/c3ay41160e.

Neff, J.C., Finlay, J.C, Zimov, S.A., Davydov, S.P., Carrasco, J.J., Schuur, E.A.G., and Davydova, A.I. 2006. Seasonal changes in the age and structure of dissolved organic carbon in Siberian rivers and streams. Geophys. Res. Lett. **33**(23): L23401, doi: 10.1029/2006GL028222.

O'Donnell, J.A., Aiken, G.R., Walvoord, M.A., and Butler, K.D. 2012. Dissolved organic matter composition of winter flow in the Yukon River basIn: implications of permafrost thaw and increased groundwater discharge. Glob. Biogeochem. Cycles. **26**(4): GB0E06.

Ohno, T. 2002. Fluorescence inner-filtering correction for determining the humification index of dissolved organic matter. Environ. Sci. Technol. **36**(4): 742–746. doi: 10.1021/es0155276.
Olefeldt, D., Turetsky, M., and Blodau, C. 2013. Altered composition and microbial versus UV-mediated degradation of dissolved organic matter in boreal soils following wildfire. Ecosystems. **16**(8): 1396–1412. doi: 10.1007/s10021-013-9691-y.
Parlanti, E., Wörz, K., Geoffroy, L., and Lamotte, M. 2000. Dissolved organic matter fluorescence spectroscopy as a tool to estimate biological activity in a coastal zone submitted to anthropogenic inputs. Org. Geochem. **31**(12): 1765–1781. doi: 10.1016/S0146-6380(00)00124-8.
Pautler, B.G., Simpson, A.J., McNally, D.J., Lamoureux, S.F., and Simpson, M.J. 2010. Arctic permafrost active layer detachments stimulate microbial activity and degradation of soil organic matter. Environ. Sci. Technol. **44**(11): 4076–4082. doi: 10.1021/es903685j.
R Core Team. 2013. R: a language and environment for statistical computing. R Foundation for Statistical Computing, Vienna, Austria. http://www.R-project.org.
Raymond, P.A., McClelland, J.W., Holmes, R.M., Zhulidov, A.V., Mull, K., Peterson, B.J., Striegl, R.G., Aiken, G.R., and Gurtovaya, T.Y. 2007. Flux and age of dissolved organic carbon exported to the Arctic Ocean: a carbon isotopic study of the five largest arctic rivers. Glob. Biogeochem. Cycles. **21**(4): GB4011
Schmidt, M.W.I., Torn, M.S., Abiven, S., Dittmar, T., Guggenberger, G., Janssens, I.A., Kleber, M., Kogel-Knabner, I., Lehmann, J., et al. 2011. Persistence of soil organic matter as an ecosystem property. Nature. **478**(7367): 49–56. doi: 10.1038/nature10386.
Schuur, E.A.G., McGuire, A.D., Schadel, C., Grosse, G., Harden, J.W., Hayes, D.J., Hugelius, G., Koven, C.D., Kuhry, P., et al. 2015. Climate change and the permafrost carbon feedback. Nature. **520**(7546): 171–179. doi: 10.1038/nature14338.
Spencer, R.G.M., Aiken, G.R., Wickland, K.P., Striegl, R.G., and Hernes, P.J. 2008. Seasonal and spatial variability in dissolved organic matter quantity and composition from the Yukon River basin, Alaska. Glob. Biogeochem. Cycles. **22**(4): GB4002.
Spencer, R.G.M., Aiken, G.R., Butler, K.D., Dornblaser, M.M., Striegl, R.G., and Hernes, P.J. 2009. Utilizing chromophoric dissolved organic matter measurements to derive export and reactivity of dissolved organic carbon exported to the Arctic Ocean: a case study of the Yukon River, Alaska. Geophys. Res. Lett. **36**(6): L06401, doi: 10.1029/2008GL036831.
Spencer, R.G.M., Mann, P.J., Dittmar, T., Eglinton, T.I., McIntyre, C., Holmes, R.M., Zimov, N., and Stubbins, A. 2015. Detecting the signature of permafrost thaw in Arctic rivers. Geophys. Res. Lett. **42**(8): 2830–2835. doi: 10.1002/2015GL063498.
Stedmon, C.A., and Bro, R. 2008. Characterizing dissolved organic matter fluorescence with parallel factor analysis: a tutorial. Limnol. Oceanogr. **6**(11): 572–579. doi: 10.4319/lom.2008.6.572.
Stedmon, C.A., Markager, S., and Bro, R. 2003. Tracing dissolved organic matter in aquatic environments using a new approach to fluorescence spectroscopy. Mar. Chem. **82**(3–4): 239–254. doi: 10.1016/S0304-4203(03)00072-0.
Striegl, R.G., Aiken, G.R., Dornblaser, M.M., Raymond, P.A., and Wickland, K.P. 2005. A decrease in discharge-normalized DOC export by the Yukon River during summer through autumn. Geophys. Res. Lett. **32**(21): L21413, doi: 10.1029/2005GL024413.
Vonk, J.E., Mann, P.J., Davydov, S., Davydova, A., Spencer, R.G.M., Schade, J., Sobczak, W.V., Zimov, N., Zimov, S., et al. 2013*a*. High biolability of ancient permafrost carbon upon thaw. Geophys. Res. Lett. **40**(11): 2689–2693. doi: 10.1002/grl.50348.
Vonk, J.E., Mann, P.J., Dowdy, K.L., Davydova, A., Davydov, S.P., Zimov, N., Spencer, R.G.M., Bulygina, E.B., Eglinton, T.I., and Holmes, R.M. 2013*b*. Dissolved organic carbon loss from Yedoma permafrost amplified by ice wedge thaw. Environ. Res. Lett. **8**(3): 035023, doi: 10.1088/1748-9326/8/3/035023.
Vonk, J.E., Tank, S.E., Mann, P.J., Spencer, R.G.M., Treat, C.C., Striegl, R.G., Abbott, B.W., and Wickland, K.P. 2015. Biodegradability of dissolved organic carbon in permafrost soils and waterways: a meta-analysis. Biogeosci. Discuss. **12**(11): 8353–8393. doi: 10.5194/bgd-12-8353-2015.
Walker, S.A., Amon, R.M.W., and Stedmon, C.A. 2013. Variations in high-latitude riverine fluorescent dissolved organic matter: a comparison of large Arctic rivers. J. Geophys. Res. **118**(4): 1689–1702. doi: 10.1002/2013JG002320.
Ward, C.P., and Cory, R.M. 2015. Chemical composition of dissolved organic matter draining permafrost soils. Geochim. Cosmochim. Acta. **167**: 63–79. doi: 10.1016/j.gca.2015.07.001.
Weishaar, J.L., Aiken, G.R., Bergamaschi, B.A., Fram, M.S., Fujii, R., and Mopper, K. 2003. Evaluation of specific ultraviolet absorbance as an indicator of the chemical composition and reactivity of dissolved organic carbon. Environ. Sci. Technol. **37**(20): 4702–4708. doi: 10.1021/es030360x.
Wickland, K.P., Aiken, G.R., Butler, K., Dornblaser, M.M., Spencer, R.G.M., and Striegl, R.G. 2012. Biodegradability of dissolved organic carbon in the Yukon River and its tributaries: aeasonality and importance of inorganic nitrogen. Glob. Biogeochem. Cycles. **26**(4): GB0E03.
Woods, G.C., Simpson, M.J., Pautler, B.G., Lamoureux, S.F., Lafrenière, M.J., and Simpson, A.J. 2011. Evidence for the enhanced lability of dissolved organic matter following permafrost slope disturbance in the Canadian High Arctic. Geochim. Cosmochim. Acta. **75**(22): 7226–7241. doi: 10.1016/j.gca.2011.08.013.